Dysfunctional Hippocampal-Prefrontal Network Underlies a Multidimensional Neuropsychiatric Phenotype following Early-Life Seizure

Running head: HPC-PFC dysfunction and early-life seizure

Rafael Naime Ruggiero[1*], Danilo Benette Marques[1#], Matheus Teixeira Rossignoli[1#], Jana Batista De Ross[1], Tamiris Prizon[1], Ikaro Jesus Silva Beraldo[2,3], Lezio Soares Bueno-Junior[4], Ludmyla Kandratavicius[5], Jose Eduardo Peixoto-Santos[6], Cleiton Lopes Aguiar[2,3], João Pereira Leite[1*].

[1]Department of Neuroscience and Behavioral Sciences, Ribeirão Preto Medical School, University of São Paulo, Ribeirão Preto, São Paulo, Brazil.
[2]Department of Physiology and Biophysics Federal University of Minas Gerais, Belo Horizonte, Minas Gerais, Brazil.
[3]Laboratory of Molecular and Behavioral Neuroscience (LANEC), Federal University of Minas Gerais, Belo Horizonte, Brazil
[4]Department of Psychiatry, University of Michigan Medical School, Ann Arbor, Michigan, USA
[5]Department of Pathology, State University of Campinas, Campinas, São Paulo, Brazil
[6]Neuroscience Discipline, Department of Neurology and Neurosurgery, Universidade Federal de São Paulo, São Paulo, Brazil

***Corresponding author:** rafaruggiero@gmail.com, jpleite@fmrp.usp.br
[#]DBM and MTR contributed equally to this work

Conflict of interest

The authors declare no competing financial interests.

Acknowledgements

This research was funded by Fundação de Amparo à Pesquisa do Estado de São Paulo - FAPESP (R.N.R.: 2018/02303-4; M.T.R.: 2020/01510-6; D.B.M.:

2022/16812-3; J.P.L.: 2016/17882-4), Coordenação de Aperfeiçoamento de Pessoal de Nível Superior - CAPES - Finance Code 001 (D.B.M.: 88882.328283/2019-01), and Conselho Nacional de Desenvolvimento Científico e Tecnológico - CNPq (J.P.L.: 305104/2020-9 and 422911/2021-6; T.P.: 164165/2018-5). We thank Renato Meirelles e Silva, Renata Caldo Scandiuzzi and Daniela Ribeiro for technical support. We thank Ana Carolina Medeiros and Rafael D'Agosta for helping with the photomicrography and histology. We also thank Patrick Forcelli, Claudio Queiroz, Marcelo Caetano, Tonicarlo Velasco, Ricardo Saute and Norberto Garcia Cairasco for discussions. RNR and JPL designed the research. RNR, CLA and LSBJ developed the methodology. RNR, DBM, TP and MTR conducted the experiments. RNR, DBM, and IJSB analyzed data. MTR edited the figures. JBDR, LK, TP and JEPS performed immunohistochemistry. TP and JEPS conducted the neurochemistry experiments. JPL supervised the project. All authors wrote and revised the manuscript.

Abstract

Brain disturbances during development can have a lasting impact on neural function and behavior. Seizures during this critical period are linked to significant long-term consequences such as neurodevelopmental disorders, cognitive impairments, and psychiatric symptoms, resulting in a complex spectrum of multimorbidity. The hippocampus-prefrontal cortex (HPC-PFC) circuit emerges as a potential common link between such disorders. However, the mechanisms underlying these outcomes and how they relate to specific behavioral alterations are unclear. We hypothesized that specific dysfunctions of hippocampal-cortical communication due to early-life seizure would be associated with distinct behavioral alterations observed in adulthood. Here, we performed a multilevel study to investigate behavioral, electrophysiological, histopathological, and neurochemical long-term consequences of early-life *Status epilepticus* in male rats. We show that adult animals submitted to early-life seizure (ELS) present working memory impairments and sensorimotor disturbances, such as hyperlocomotion, poor sensorimotor gating, and sensitivity to psychostimulants despite not exhibiting neuronal loss. Surprisingly, cognitive deficits were linked to an aberrant increase in the HPC-PFC long-term

potentiation (LTP) in a U-shaped manner, while sensorimotor alterations were associated with heightened neuroinflammation, as verified by glial fibrillary acidic protein (GFAP) expression, and altered dopamine neurotransmission. Furthermore, ELS rats displayed impaired HPC-PFC theta-gamma coordination and an abnormal brain state during active behavior resembling rapid eye movement (REM) sleep oscillatory dynamics. Our results point to impaired HPC-PFC functional connectivity as a possible pathophysiological mechanism by which ELS can cause cognitive deficits and psychiatric-like manifestations even without neuronal loss, bearing translational implications for understanding the spectrum of multidimensional developmental disorders linked to early-life seizures.

Introduction

The early years of life represent a critical period for neuronal maturation and the development of cognitive functions (Short and Baram, 2019). Disturbances during this period can have a lasting impact on neuronal activity and cause multifaceted neuropsychiatric manifestations (Marín, 2016). Seizures are a prevalent disturbance in the immature brain and are often associated with profound and enduring adverse neurological outcomes that persist throughout adulthood (Brunquell et al., 2002; Holmes, 2009). Children who experience early-life seizures (ELS) not only face an increased likelihood of developing epilepsy but also have a heightened susceptibility to cognitive impairments and behavioral disorders, including autism spectrum disorder (ASD), attention deficit hyperactivity disorder (ADHD), intellectual disability, and psychiatric symptoms like schizophrenia (Dreier et al., 2019; Holmes, 2009; Kaufmann et al., 2009). Since the pathophysiological mechanisms linking ELS and neurodevelopmental disorders are complex, understanding how ELS *per se* affects neuronal function and dissecting the associations between neurobiological and behavioral alterations are crucial for developing better treatments for these conditions.

In experimental models, ELS induces long-term cognitive and behavioral alterations with translational validity with the main neuropsychiatric domains affected in humans (Holmes, 2016). Studies have reported that a prolonged ELS in rodents can lead to cognitive deficits, increased anxiety, reduced social interaction, and facilitated development of epilepsy (Castelhano et al., 2013; De

102 Oliveira et al., 2008a; Kubova et al., 2004). Interestingly, ELS models do not
103 exhibit severe neuronal loss or structural damage (Baram et al., 2002; Sinh et al.,
104 2003), suggesting that the behavioral alterations induced by ELS may be
105 mediated by functional and molecular effects at the brain circuit level
106 (Kandratavicius et al., 2012b, 2012a). The hippocampal-prefrontal cortical circuit
107 (HPC-PFC) plays a crucial role in cognitive and sensorimotor processes, and
108 evidence converges to indicate its dysfunction as a possible common mechanism
109 shared between ELS, neurodevelopmental, and psychiatric disorders, especially
110 epilepsy, psychosis/schizophrenia, ASD, and cognitive disability (Ruggiero et al.,
111 2021; Sigurdsson and Duvarci, 2016). Reports indicate that ELS impacts HPC-
112 PFC functional connectivity, as revealed by the coordination of network
113 oscillations during particular situations (Barry et al., 2020; Kleen et al., 2011;
114 Mouchati et al., 2019; Niedecker et al., 2021). However, how specific functional
115 or molecular effects of ELS on the HPC-PFC network are associated with
116 separate behavioral dimensions within this complex multimorbidity spectrum
117 remains unknown. Also, since behavioral alterations of ELS are long-lasting and
118 progressive, a comprehensive characterization of network dynamics across brain
119 states would be pivotal for a complete understanding of the effects of ELS on
120 brain function.

121 Here, we hypothesized that ELS would produce long-term alterations in
122 HPC-PFC neuronal dynamics related to behavioral abnormalities (Ruggiero et
123 al., 2012). To test this hypothesis, we induced *Status epilepticus* (SE) as a model
124 of prolonged ELS and performed behavioral tests to assess cognitive and
125 sensorimotor processes. Then, we performed neurophysiological,
126 immunohistochemical, and neurochemical experiments to study potential
127 changes in the HPC-PFC circuits that could underlie such behavioral alterations.
128 We found that adult ELS rats present a myriad of behavioral impairments: working
129 memory deficits, hyperlocomotion, poor sensorimotor gating, and behavioral
130 sensitivity to psychostimulants. Surprisingly, we found an enhanced long-term
131 potentiation (LTP) in the HPC-PFC pathway of ELS animals correlated with
132 cognitive impairment in a U-shaped manner. Our results also describe
133 neuroinflammation and alterations in dopaminergic neurotransmission as
134 significant contributors to sensorimotor disturbances. We also investigated HPC-
135 PFC dynamics across different brain states in freely-moving rats. ELS rats

displayed an increased HPC theta power and impaired coordination of PFC gamma activity during active behavior. During rapid eye movement (REM) sleep, ELS rats showed a reduction in HPC-PFC coherence. Remarkably, ELS rats displayed an aberrant brain state during active behavior characterized by oscillatory dynamics oddly similar to REM sleep. Finally, we implemented a linear discriminant model, demonstrating that collective patterns of oscillatory alterations accurately distinguished ELS from control animals. Interestingly, although these alterations relate to broad clinical manifestations of neurodevelopmental disturbances and psychiatric manifestations, we recognize a particular convergence of dysfunctional patterns at multiple levels linking the consequences of ELS to functional alterations reported in animal models of epilepsy, psychosis/schizophrenia, ASD, and cognitive disability. These convergent patterns indicate that epileptogenic processes triggered during early life, such as neuroinflammation, could lead to altered neurotransmission and, consequently, aberrant dynamics in the HPC-PFC coordination, potentially contributing to the neurological and psychiatric manifestations linked to early-life seizure.

Materials and Methods

Animals

Wistar rats were housed in a colony room with controlled temperature (22 ± 2 °C) and a 12-h light/dark cycle with free access to food and water. Litters contained up to 8 animals with a maximum of 5 males. Rats were weaned at 21 days postnatally (P21). All procedures were performed according to the National Council for the Control of Animal Experimentation guidelines for animal research and approved by the local Committee on Ethics in the Use of Animals (Ribeirão Preto Medical School, University of São Paulo; protocol: 159/2014).

Experimental Designs

We used four cohorts (a total of 17 litters) to compare the effects of early-life *Status Epilepticus* (ELS) *versus* control (CTRL) animals. The first cohort was used for acute electrophysiology during the induction of ELS (n=5, ELS only). Importantly, this group was utilized solely for the purpose of confirming that the

169 SE protocol induced behavioral and electrophysiological ictal activity. This group
170 was not subjected to any additional statistical tests or data analyses. The second
171 cohort was used for behavioral tests (CTRL n=11, and ELS n=14), synaptic
172 plasticity experiments (CTRL n=7, and ELS n=7), and immunohistochemistry
173 (CTRL n=9, and ELS n=11). The reduction in sample size for LTP and
174 immunohistochemistry experiments was influenced by practical challenges,
175 including mortality during LTP surgery and issues related to tissue damage or
176 loss during the immunohistochemical protocol. The third cohort was used to
177 investigate HPC-PFC dynamics in freely moving rats (CTRL n=6, and ELS n=9).
178 Finally, in the fourth cohort, we assessed behavioral sensitization to
179 psychostimulants (CTRL n=15, and ELS n=14) and neurochemical quantification
180 (CTRL n=8, and ELS n=9). The reduced sample size for neurotransmitter
181 analysis was a deliberate selection of a subsample, considering the complexity
182 and cost associated with the neurotransmitter quantification protocol. Rats were
183 randomly selected for each group.
184
185 ***Early-Life Status Epilepticus***
186 At P11-P12 we induced a 2-hour SE using lithium chloride (LiCl, 127
187 mg/kg, i.p., Sigma-Aldrich, USA) 18-20 hours prior to injection of
188 methylscopolamine (1 mg/kg, i.p., Sigma-Aldrich) and pilocarpine (80 mg/kg, s.c.,
189 Sigma-Aldrich, USA) (Kubová and Mareš, 2013). Behavioral seizures were
190 monitored following the Racine scale (Racine, 1971). SE was interrupted by
191 diazepam (5 mg/kg, i.p., Teuto, Brazil) at the 2-hour mark. During the recovery
192 period (1 week post-ELS) we provided food supplementation and subcutaneous
193 rehydration with saline and monitored body temperature and weight.
194
195 ***Behavior***
196 The radial-arm maze working memory task was based on Floresco et al.
197 (1997). Briefly, rats were kept at 85-90% of their initial body weight throughout
198 the 21 days of the experiment. Training consisted of single daily sessions, each
199 one divided into the training phase and test phase, 30 min apart. During the
200 training session, four doors were kept open providing access to food pellets. In
201 the test session, all doors remained open, but with pellets available only in the
202 four arms that were closed in the previous training session. The sessions were

203 terminated upon full pellet consumption or after 5 min. Two types of errors were
204 quantified: Reference error: reentering arms previously visited during the training
205 session; Working memory error: reentering an arm already visited during the test
206 session. The sum of both categories denoted the total errors for each animal.

207 Three days after returning to *ad libitum* diet, locomotor activity was
208 evaluated for 30 min in the open field test (Wolf et al., 2016).

209 Immediately after the open field test, rats were examined for prepulse
210 inhibition (PPI) of the acoustic startle. The PPI test consisted of a habituation
211 period (5 min) followed by 72 trials (intertrial interval: 15 ± 8 s) with prepulse alone
212 (PP), startling pulse alone (P), prepulse followed by a startling pulse (PP + P),
213 and no stimulus, all of which accompanied by background noise (65 dB white
214 noise). Startle-eliciting stimuli were presented at 120 dB for 40 ms (P) and
215 prepulse stimuli were presented for 20 ms (PP, 1000 Hz; 71, 77, and 83 dB; 20
216 ms). Trials were presented in a random order, with each trial type being presented
217 six times. We used the equation: %PPI = 100 − 100 × (mean startle amplitude at
218 PP + P)/(mean startle amplitude at P) (Wolf et al., 2016).

219 In order to measure the effects of ELS on sensitization to
220 psychostimulants, we performed the apomorphine-induced locomotion test. At
221 P80-90, rats were placed in the open field apparatus and were allowed to roam
222 for 60 min. Then, we injected apomorphine (APO, 1.5 mg/kg, i.p., Sigma-Aldrich,
223 USA) and measured locomotion for another 60 min. The distance across blocks
224 was normalized by Z-score to the mean of baseline blocks.

225

226 ***Synaptic Plasticity***

227 HPC-PFC synaptic plasticity studies were performed as described in
228 previous works from our group (Bueno-Junior et al., 2018; Ruggiero et al., 2018).
229 Briefly, rats were anesthetized with urethane (1.2 mg/Kg in NaCl 0.15 M, i.p.) for
230 electrode implantation. A recording electrode (Teflon-coated tungsten wires 60
231 μm, AM-Systems) was inserted in the medial PFC (prelimbic region (PL),
232 anterior-posterior: 3.0 mm; medial-lateral, ML: 0.5 mm; dorsal-ventral, DV: 3.2
233 mm), and a bipolar stimulation electrode (twisted wires; ~500 μm inter-pole
234 distance) was inserted in the ipsilateral HPC (intermediate CA1 AP: −5.6 mm;
235 ML: 4.5 mm; DV: 2.5 mm). An additional burr hole was drilled over the right

236 parietal cortex for a reference screw. Temperature was kept constant at 37 ±
237 0.5°C during the experiment.
238 HPC was stimulated with single monophasic pulses (200 μs, 0.05 Hz,
239 150–300 μA, 80-ms inter-pulse interval) while recording PFC field postsynaptic
240 potentials (fPSPs). Stimulation intensity (60–500 μA) was calibrated to evoke 50–
241 60% of the maximal fPSP amplitude. Field recordings were conditioned through
242 a preamplifier (100× gain, 0.03–3 kHz bandpass; Grass) and digitized at 10 kHz
243 (ADInstruments). For LTP induction, we used a high-frequency stimulation (HFS)
244 protocol consisting of 2 series (10 min apart) of 10 trains (0.1 Hz), each train with
245 50 pulses at 250 Hz (Ruggiero et al., 2018). fPSP amplitudes and slopes were
246 computed as the difference and slope between the positive and negative peaks,
247 respectively. Short-term synaptic plasticity was estimated by paired-pulse
248 facilitation (PPF), calculated as the ratio of the fPSP2 and fPSP1 (Lopes-Aguiar
249 et al., 2020). Amplitudes and slopes were normalized as ratios of the baseline
250 mean and averaged into 10-min bins.
251
252 ***Brain Tissue Processing***
253 *Immunohistochemistry*
254 We employed a standardized immunohistochemistry protocol (Peixoto-
255 Santos et al., 2015) to estimate NeuN+ neuronal density and to evaluate
256 parvalbumin-expressing (PV) interneurons, mGluR5 expression, and glial
257 fibrillary acid protein (GFAP) reaction. Briefly, endogenous peroxidases were
258 blocked and the antigens were exposed by microwave-induced retrieval. We
259 used the primary antibodies against NeuN (Chemicon, USA; 1:1000), PV
260 (Calbiochem, USA; 1:500), mGluR5 (Millipore, USA; 1:200), and GFAP (Dako,
261 Denmark; 1:500) proteins, and biotinylated secondary antibodies (Dako,
262 Denmark; 1:200). Revelation was performed with Elite ABC Kit (Vector) and
263 diaminobenzidine solution (Pierce).
264 Images from the regions of interest were captured at 200× magnification
265 in the Axio Scope.A1 microscope system (Carl Zeiss). The regions of interest
266 included the hippocampus (CA1 and GL, granule layer of dentate gyrus),
267 entorhinal cortex (EC), infralimbic (IL) and prelimbic cortex (PL), and thalamic
268 reticular nucleus (TRN). Images were then processed in Image J software (NIH,

269 USA; 1.48v). Data are shown as the density of NeuN positive cells and
270 immunopositive area for PV, mGluR5, and GFAP.
271
272 *High-Performance Liquid Chromatography (HPLC)*
273 Samples were taken bilaterally from the nucleus accumbens (NAc), PFC,
274 and HPC. The samples were homogenized with ultrasound in a 0.1 mol/L $HClO_4$
275 0.02% $Na_2S_2O_2$ solution containing dihydroxybenzylamine (DHBA, 146.5 ng/mL),
276 and homoserine (HSER, 10 µg/mL) as internal standards and at a dilution of 15
277 µL per sample milligram. We employed Shimadzu LC-10AD isocratic systems
278 with a fluorescence detector for glutamate (Glu) and gamma-aminobutyric acid
279 (GABA), and an electrochemical detector for dopamine (DA) and its metabolites
280 3,4-dihydroxyphenylacetic acid (DOPAC) as previously published (Castro-Neto
281 et al., 2013). The neurotransmitter levels were considered to reflect
282 neurotransmitter stock in synaptic vesicles, their metabolites reflected the
283 release, and metabolite/neurotransmitter ratios were taken as an index of
284 neurotransmitter turnover. Standards containing all amino acids and
285 monoamines/metabolites of interest were employed to define their respective
286 peaks in the samples.
287
288 ***Freely Moving Electrophysiology***
289 *Electrophysiological recordings*
290 Chronic head caps consisted of two eight-channel connectors (Omnetics),
291 one for the PFC (PL, 7 wires) and another for the HPC (intermediate CA1, 7 wires)
292 (Bueno-Junior et al., 2017; Marques et al., 2022). We additionally implanted a
293 recording wire into the trapezius muscle to serve as an electromyogram (EMG).
294 The EMG wire was soldered to the HPC connector. Microscrews were fastened
295 into the skull, including a ground reference in the intraparietal area. Animals were
296 allowed to recover for 8-9 days before recordings.
297 To record electrophysiological signals through sleep-wake states, rats
298 were placed into a shuttle box apparatus inside a soundproof box with food and
299 water *ad libitum*. Recordings varied between 30 to 48 hours, divided later into
300 periods of 6 hours for analysis. Local field potentials (LFP) were recorded through
301 a multichannel acquisition processor (Plexon) (1000× gain, 0.7-500 Hz bandpass
302 filter, 1-kHz sampling rate).

Classification of sleep-wake states

Classification of the sleep-wake cycle states was carried out through a semi-supervised machine learning pipeline. The HPC theta (4.5-12 Hz), PFC delta (0.7-4 Hz), and EMG (100-200 Hz) power were computed in 5-second epochs without overlaps (4 tapers; time-bandwidth product: 2.5). A support vector machine (SVM) (radial basis function) was trained to discriminate the epochs into: (1) awake or sleep epochs using EMG power; (2) REM or NREM epochs based on theta/delta ratio; (3) quiet wake (QWK) or active (ACT) epochs based on theta/delta ratio. Later, we classified our recordings based on 30-second epochs by grouping sets of six 5-second epochs and considering the most representative state.

Spike wave-discharge detection (SWD)

For spike wave-discharge detection, we used the PFC recordings. First, the short-time Fourier transform (STFT) was computed within 3-70 Hz throughout 250-ms windows with 50% overlap. A detection threshold was defined as the mean + 1.5 standard deviation of the absolute value of the STFT of the frequency bands 4.4-16.4, 17.6-32.8, and 35.1-55 Hz throughout the entire recording. SWD events were detected when the average STFT of the aforementioned frequency bands at one epoch exceeded the threshold. Consecutive epochs above the threshold were grouped as the same event. The beginning and the end of an event were defined as the closest epochs when the average STFT was lower than the mean + 1 standard deviation of STFT of the frequency bands of interest. Lastly, the detected putative events were manually sorted by an expert.

Spectral estimates

We divided 30-s epochs into 3-s epochs for spectral analyses. Power spectrum densities (PSD) and magnitude-squared coherence were obtained using Welch's method with 1-s segments, 50% overlap, and Hamming windowing. Relative power was obtained by dividing values by the sum within 0.5-55 Hz for each epoch. We defined the frequency bands: delta (1-4 Hz), theta (4.5-11 Hz), low gamma (30-55 Hz), and high-gamma (65-100 Hz) to compare

336 estimates and obtained the spectral peak of each epoch using MATLAB function
337 *findpeaks*.
338 To quantify theta oscillation power we used the FOOOF algorithm
339 (Donoghue et al., 2020), which parametrizes the PSD separating the periodic and
340 aperiodic components of the signal. We used frequencies within 3-40 Hz, the
341 "fixed" aperiodic mode, a minimum peak height of 0.05, and a maximum number
342 of peaks of 4 (https://fooof-tools.github.io/fooof/). EMG data were low-cut filtered
343 (>30 Hz) and the sum of power within 30-200 Hz was obtained.
344 As a synchrony measure, we also computed cross-correlations between
345 each pair of LFPs (low-pass filter of 50 Hz) recorded from the HPC and PFC using
346 a maximum lag of 1 s. Coefficients were normalized so that the autocorrelations
347 at zero lag were one. We observed that the highest coefficients occurred in the
348 range of -80 to -20 ms (HPC leading the PFC), so we obtained the maximum
349 coefficient within this range for each rat average for comparisons. Cross-
350 spectrum power was calculated using Welch's method for the normalized
351 correlation coefficients from -1 to 1 s.
352 For cross-frequency amplitude spectrum correlations, we computed the
353 absolute STFT for each 3-s epoch throughout 100-ms segments with 50%
354 overlap and Hamming windowing across 0.5-Hz frequency bins within 0.5-200
355 Hz. We calculated the correlation matrix for each frequency pair using Pearson's
356 R.
357
358 *State maps*
359 After state classification and spectral analysis, we computed two-
360 dimensional state maps to investigate the natural distinction between sleep-wake
361 states. The state maps were computed according to Gervasoni et al. (2004) and
362 Dzirasa et al. (2006). First, we obtained the power *ratio 1* (4.5-9/4.5-50 Hz) and
363 *ratio 2* (2-20/2-50 Hz) for each region and the first principal component, estimated
364 by singular value decomposition algorithm considering both regions, for each
365 ratio. Finally, we applied a Hann window of 10 epochs on scores throughout time
366 for smoothing.
367 To identify the intermediate states (IS), we first estimated the trajectory
368 *speed* of epochs throughout state map dimensions as the Euclidean distance
369 between each epoch and its predecessor. Then, we defined a threshold of 0.1

and labeled the epochs with greater speed as IS. This threshold was determined heuristically, corresponding closely to the expected value plus a standard deviation from a Poisson distribution across rats.

From visual inspection and the literature (Dzirasa et al., 2006; Gervasoni et al., 2004), the state maps usually separate three well-defined clusters heuristically corresponding to awake, REM, and NREM sleep. To assure the correspondence between state map clusters and the classification outcomes, we performed Gaussian mixture models clustering of the state maps for 3 clusters and 80% posterior probabilities and computed Chi-squared tests with the classified NREM, REM, and awake (QWK+ACT) labels. Three animals were excluded for having outlier lower Chi-values. Although QWK and ACT states are often evenly distributed inside the awake cluster, QWK epochs may overlap with intermediate states closer to NREM, so the ACT epochs were considered to represent more precisely the localization of neural dynamics associated with behavior in the state map. The dissimilarity between ACT and REM states was estimated by the average pairwise state map Euclidean distance of all epochs between the two states.

We used machine learning algorithms to decode sleep-wake states from the state map. We used the ACT and REM state map *ratios 1* and *2* values. We applied a linear and radial basis function SVM *fictcsvm* function in MATLAB ('KernelFunction', 'linear' or ‘rbf’) as well as a Random Forest algorithm using the *fitcensemble* function in MATLAB ('Method', 'bag', 'NumLearningCycles', 50, for Random Forest) to decode states. We used the ACT and REM epochs from all the rats creating one single model for the CTRL or ELS condition. Using the same approach, we also constructed a random forest decoder model with non-reduced variables using 1 to 55 Hz (0.5 Hz bins) for the PFC and HPC power and coherence. Discrimination was evaluated using the area under the receiver operating characteristic curve (AUC-ROC). The pointwise confidence interval was calculated using a 1000-repetition bootstrap. Average AUC-ROC values were calculated using the prediction of the trained model on 20% of the epochs as test data and repeating the process 100 times.

Statistical Analysis

Data were analyzed using GraphPad Prism Software version 9.00 (GraphPad Software, LLC), and R studio version 2021. We used paired Student *t*-tests for within-group comparisons and two-sample *t*-tests for between-group comparisons. Two-way ANOVA with repeated measures (RM) was performed for comparisons across time bins, using Sidak's multiple comparison test as a *post-hoc*. To examine linear model assumptions, we analyzed the distribution of the residuals using a Q-Q plot, the Kolmogorov-Smirnov test, homoscedasticity, and the residual plot. We used the Mann-Whitney test to compare two groups and the Wilcoxon signed-rank test to paired comparisons as non-parametric alternatives. We calculated Pearson's linear correlation and Spearman's rank correlation as a nonparametric equivalent. To compare correlation and spectral coherence estimates we applied Fisher's Z transform to the data. For multiple comparisons in the neurochemical quantification, we performed Holm's procedure for multiple comparisons correction across neurotransmitters and metabolites per region.

Data are expressed as the mean ± SEM. The significance level was set to 0.05 unless stated otherwise. For some multiple comparisons, statistical values are expressed as the range. Significances are expressed as $^{\dagger}p < 0.1$, $^{*}p < 0.05$, $^{**}p < 0.01$, and $^{***}p < 0.001$.

Linear mixed-effects models

We also constructed statistical inferential models across time controlling for individual variability and litter using linear mixed-effects models. We compared power and coherence estimates throughout time by dividing the electrophysiological recording into 5 periods (6 hours). Group and time (periods) were assigned as fixed effects and subject, litter, and time were assigned as random effects. We used this approach to construct a maximal random effects structure model as preconized in the literature as more generalizable (Barr et al., 2013). The model was estimated by restricted maximum likelihood using the *lme* function of the *nlme* package (Pinheiro et al., 2023) with an unstructured covariance matrix.

Multivariate analysis

Each variable was Z-scored before multivariate analysis. We constructed correlograms to assess the relationship within behavioral and neurobiological

437 measures. Variables were sorted by agglomerative hierarchical clustering using
438 Ward's method and correlation as the metric. We also performed agglomerative
439 hierarchical clustering of subjects using Ward's method and Euclidean distance
440 as the metric to assess how unsupervised clustering by our multivariate data
441 might match the experimental groups. An optimal number of clusters was
442 estimated using the silhouette method and final definition was based on
443 parsimonious interpretability of the results.

444 Principal component analysis (PCA), using singular-value decomposition,
445 was used for dimensionality reduction to find collective patterns of variance within
446 behavioral variables (behavior factors) and neurobiological variables
447 (neurobiology factors), and to reduce each immunohistochemical measure
448 across all brain regions into single scores (Johnson and Wichern, 2007; Marques
449 et al., 2023, 2022). Principal components (PCs) were projected onto data and the
450 mean score was compared between conditions.

451 Canonical correlation analysis (CCA) was performed to describe
452 multivariate relationships between behavioral and neurobiological measures
453 (Drysdale et al., 2017). Missing data were imputed using the multiple imputation
454 by chained equations algorithm. For CCA, we used the first PC (PC1) and second
455 PC (PC2) of behavioral variables as inputs for the behavioral factors and the PC1
456 of each immunohistochemical variable (NeuN, PV, mGluR5, and GFAP,) across
457 all brain regions and the Z-scored LTP data as inputs for the neurobiological
458 factors. Variables were narrowed down from 30 to 7, which is statistically
459 appropriate for our sample size. We used the CCA package in R to obtain the
460 canonical dimensions and performed the Hotelling-Lawley trace statistic to
461 assess the significance of each dimension.

462 We used multivariate generalized linear models (GLM) with a Gaussian
463 family and an identity link function. Quasi-Poisson regression (quasi-Poisson
464 family and logarithmic link function) were used for count data with overdispersion
465 (Errors in the radial maze) using a quadratic covariate (LTP). We constructed two
466 types of models: 1) a full model considering all the covariates; and 2) a restricted
467 model using backward stepwise model selection based on the Akaike information
468 criterion.

469 To assess the effectiveness of neurophysiological features in
470 discriminating CTRL from ELS rats, we fitted a regularized linear discriminant

classifier model on the PCA scores of selected electrophysiological variables. We used the MATLAB function *fitcdiscr* without hyperparameter optimization (Johnson and Wichern, 2007; Marques et al., 2023, 2022). The linear classifier using two predictors allowed the graphical representation and avoided the overfitting of a high number of variables. Accuracy was determined as the probability of correct category assignments using leave-one-out cross-validation. We also determined the contribution of each original neurophysiological variable by assessing their respective AUCs using a univariate logistic regression model.

Results

ELS induces cognitive and behavioral impairments in adulthood

SE induced by lithium-pilocarpine in early life (Fig. 1A) produced an unequivocal and stereotyped seizure, consisting mainly of forelimb myoclonus and orofacial automatism (Racine 3), with some animals showing further development into bilateral forelimb myoclonus, rearing and falling (Racine 4 and 5) (Racine, 1971). Seizures were confirmed electrophysiologically in freely moving recordings of the frontal cortex and HPC, with paroxysms starting 10 min after pilocarpine injection and persisting for at least 120 min (Fig. 1B).

Next, we hypothesized that ELS rats would display a wide range of long-term cognitive and sensorimotor consequences. Therefore, we submitted the animals to several behavioral tests. (Fig. 2A). First, we evaluated possible weight differences as a confounder of behavioral measures. ELS rats displayed weight loss on the day after SE (Two-way RM ANOVA, treatment effect: $F_{(9,207)}$ = 11.7, $p < 0.0001$, Sidak's *post-hoc:* $p < 0.0001$; Fig. 2B). However, ELS animals recovered the pace of normal weight gain in the subsequent days (*post-hoc*: $p > 0.05$) and into adulthood (Fig. 2C), showing no distinction to CTRL before (*t*-test, $t_{(23)} = 1.440$, $p = 0.1634$) or during food restriction (*t*-test, $t_{(23)} = 0.0535$, $p = 0.9577$), indicating that behavioral effects were unrelated to weight differences or alterations in food-seeking.

Importantly, when examined for spatial memory in the radial-arm maze, ELS rats presented a specific increase in working memory errors (Mann-Whitney test, $U = 36.5$, *n(CTRL, ELS)* = 11, 14, $p = 0.0254$; Fig. 2D). We found no differences in the total reference errors (*t*-test, $t_{(23)} = 1.719$, $p = 0.0991$; Fig 2D) and in the learning curve (Two-way RM ANOVA, treatment effect: $F_{(1,23)}$ =

0.8032, p = 0.3794; Fig 2E). In addition, ELS rats exhibited significantly higher locomotion in the open field test (Mann-Whitney test, U = 27, *n(CTRL, ELS)* = 11/14, p = 0.0051; Fig. 2F). ELS rats also displayed a higher startle response (*t*-test, $t_{(23)}$ = 2.757, p = 0.011; Fig. 2G) and a deficit in sensorimotor gating represented by a reduction in PPI of the acoustic startle (Two-way RM ANOVA, treatment effect: $F_{(2,46)}$ = 19.6, p < 0.0001, Sidak's *post-hoc:* PPI 71 dB: p = 0.0017; PPI 77 dB: p = 0.1040; PPI 83 dB: p = 0.030; Fig. 2H).

Interestingly, all these behavioral alterations are described in animal models of neurodevelopmental disorders such as ASD and schizophrenia (Ey et al., 2011; Scott et al., 2018; Sigurdsson, 2016). Then, we investigated if collective patterns of behavioral alterations induced by ELS could reflect latent factors representing more comprehensive behavioral dimensions. Working memory errors in the radial-arm maze showed little correlation with the other behavioral variables, while sensorimotor variables (locomotion, startle response and sensorimotor gating) presented a strong correlation with each other. PPI exhibited a positive correlation with every intensity and a negative correlation with startle response and locomotion (Fig. 2I). We also performed PCA to extract patterns of variance between multivariate behavioral data (Fig. 2J-M). Our analysis indicated that dimensionality reduction by PCA using the first two components explained 71.32% of the variability of the data (Fig. 2J). By analyzing the loadings of the PC1, the variables that contribute more strongly (>0.5) to this dimension were: high total distance, startle reflex, and low PPI scores, indicating this component represents a latent factor of sensorimotor dysfunction. In turn, the PC2 represents the cognitive dimension of the behavioral variables, as it presents a high loading value (>0.5) for working memory errors (Fig. 2K). Finally, we found that these PCs clearly distinguished CTRL from ELS animals, which presented higher values of PC1 (PC1: *t*-test, $t_{(23)}$ = 3.9713, p = 0.0006; PC2: *t*-test, $t_{(23)}$ = 1.6466, p = 0.1132; Fig. 2L-M). These results indicate that the covariance across behavioral tests can be summarized by a latent *sensorimotor factor* (PC1) and a *cognitive factor* (PC2), representing two distinct dimensions of the ELS-induced behavioral phenotype and suggesting possibly different neurobiological bases.

Aberrant HPC-PFC synaptic plasticity in animals submitted to ELS

538 Next, we tested the hypothesis that behavioral abnormalities in ELS rats
539 could be associated with synaptic plasticity impairments of the HPC-PFC
540 pathway (Fig. 3A-C). First, we looked for ELS-related alterations in basal synaptic
541 efficacy before inducing LTP. Synaptic efficacy was assessed in terms of basal
542 fPSP amplitude and slope (amplitude: *t*-test, $t_{(12)} = 1.278$, $p = 0.2255$; slope: *t*-
543 test, $t_{(12)} = 0.5470$, $p = 0.5944$; Fig. 3D), input-output curve (fPSP amplitude as a
544 function of stimulus intensity) (Two-way RM ANOVA, treatment effect: $F_{(1,12)} =$
545 0.6596, $p = 0.4325$; Fig. 3E) and PPF curve (PPF as a function of the inter-pulse
546 interval) (Two-way RM ANOVA, treatment effect: $F_{(1,12)} = 0.3345$, $p = 0.5737$;
547 Fig. 3F). None of these measures indicated alterations in ELS when compared to
548 CTRL (Fig. 3D-F).
549 Then, we proceeded to the synaptic plasticity experiments and found that
550 ELS rats presented an abnormally augmented LTP compared to CTRL (Fig. 3G;
551 Two-way RM ANOVA, treatment effect: $F_{(1,12)} = 7.54$, $p = 0.0177$; interaction
552 effect: $F_{(26,312)} = 7.393$, $p < 0.0001$; Sidak's *post-hoc:* $p < 0.05$ for 10-60 min; *t*-
553 test, $t_{(12)} = 2.747$, $p = 0.0177$; Fig. 3G inset), despite the lack of alterations in
554 basal synaptic efficacy described above (Fig. 3D-F). Aberrant LTP in the ELS rats
555 was also observed when analyzing the fPSP slope (Two-way RM ANOVA,
556 treatment effect: $F_{(1,12)} = 4.757$, $p = 0.0498$; interaction effect: $F_{(26,312)} =$
557 4.120, $p < 0.0001$; Sidak's *post-hoc:* $p < 0.05$ for 10-40 min; Fig. 3H; *t*-test, $t_{(23)} =$
558 2.794, $p = 0.0162$; Fig. 3H inset). However, short-term plasticity measured by
559 PPF decreased during the initial 30 min of recording (Two-way RM ANOVA,
560 interaction effect: $F_{(26,312)} = 3.457$, $p < 0.0001$; Sidak's *post-hoc:* $p < 0.05$ for 20-
561 30 min; Fig. 3I), possibly reflecting a ceiling effect on fPSP amplitude after LTP
562 induction. With these results, we demonstrate that, although ELS does not affect
563 basal synaptic efficiency, it significantly increases the ability of HPC-PFC circuits
564 to undergo LTP.
565
566 **ELS induces long-term neural inflammation, but not neuronal loss**
567 We sought to investigate histopathological alterations in cortico-limbic
568 circuits that could underlie the abnormalities in behavior and HPC-PFC synaptic
569 plasticity of ELS rats (Fig. 4A). In accordance with previous findings, ELS rats did
570 not present neuronal loss when adults (Mixed-effects model, $F_{(1,12)} = 0.7683$, $p =$
571 0.3980; uncorrected Mann-Whitney test, $p = 0.1666$-0.9372; Fig. 4B). However,

572 we investigated potential immunohistochemical alterations associated with
573 epilepsy and neuropsychiatric disorders and their potential correlation with
574 functional changes. Specifically, our investigation focused on assessing the
575 status of PV interneurons, mGluR5 expression, and GFAP reaction as potential
576 indicators of underlying pathophysiological mechanisms. ELS did not produce
577 long-term effects in the expression of PV (Mixed-effects model, $F_{(1,13)} = 0.008$, $p =$
578 0.9297; uncorrected Mann-Whitney test, $p = 0.3659$-0.9307; Fig. 4C) or mGluR5
579 receptors (Mixed-effects model, $F_{(1,11)} = 0.0011$, $p = 0.9735$; uncorrected Mann-
580 Whitney test, $p = 0.2467$-0.8181; Fig. 4D). Finally, we found a strong increase in
581 neuroinflammation, verified by the marked expression of GFAP in ELS rats in all
582 regions investigated except the infralimbic cortex (Mixed-effects model, $F_{(1,18)} =$
583 5.368, $p = 0.0325$; uncorrected Mann-Whitney test, $p = 0.0067$-0.0419 for GL,
584 CA1, EC, PL, and TRN, and $p = 0.2298$ for IL; Fig. 4E). Firstly, our observations
585 confirm that relevant cognitive and behavioral impairments can manifest after
586 ELS even in the absence of substantial neuronal loss in the investigated brain
587 areas. Meanwhile, these results show that ELS produces long-term and
588 widespread brain inflammation. Noteworthy, the neuroinflammation promoted by
589 SE extends beyond the HPC-PFC circuit, also affecting thalamic nuclei,
590 suggesting a large-scale impact.
591
592 **Cognitive impairment and sensorimotor disturbances are distinctly**
593 **correlated with abnormal LTP and neuroinflammation**
594 So far, we have found that ELS promotes sensorimotor and cognitive
595 behavioral alterations parallel to inducing exaggerated HPC-PFC LTP and large-
596 scale neuroinflammation while exhibiting no significant neuronal loss and subtle
597 molecular changes. However, we still do not know how specific neurobiological
598 alterations relate to particular behavioral changes. By understanding the
599 association between behavioral and neurobiological variables, we would be able
600 to infer putative mechanisms underlying the behavioral comorbidities observed in
601 ELS animals. In this context, because neurodevelopmental insults can have
602 multifaceted and intricate outcomes, we also sought to explore multivariate and
603 non-linear associations within our data.
604 To investigate multivariate relationships between the behavioral (cognitive
605 and sensorimotor factors) and neurobiological (synaptic plasticity and

606 immunohistochemical measures) dimensions of ELS effects, we conducted CCA
607 (Fig. 5A). CCA produced a significant high-correlation model (r = 0.94, Hotteling-
608 Lawley trace test, $F\text{-}approximation_{(10,12)}$ = 3.2311, p = 0.0164; Fig. 5B) that
609 clearly separated CTRL from ELS (behavior canonical dimension, t-test, $t_{(11)}$ =
610 3.693, p = 0.0035; neurobiology canonical dimension, t-test, $t_{(11)}$ = 3.917, p =
611 0.0024; Fig. 5C). By analyzing the coefficients, we observed that the behavior
612 canonical dimension showed higher values for the sensorimotor factor, but also
613 included the cognitive factor, although at a lower degree (Fig. 5D). The
614 neurobiology canonical dimension showed a larger value for the GFAP,
615 intermediate values for LTP and PV and the lowest coefficients for NeuN and
616 mGluR5 (Fig. 5D). A similar pattern was observed when analyzing the loadings
617 for each dimension (Fig 5E). Notably, the neurobiological variables have only
618 weak correlations between them (Fig. 5F). To further dissect specific multivariate
619 relationships between behavioral and neurobiological measures, we constructed
620 generalized linear models (GLM). The GLM indicates GFAP, PV, and LTP as the
621 most significant variables that explain the sensorimotor factor variance
622 (coefficients = 2.3775, 0.8457, and 0.5187; p = 0.1164, 0.00548, 0.08474 for
623 GFAP, PV, and LTP, respectively, (Fig. 5G). Accordingly, GLM multivariate
624 regression indicates a strong association between the sensorimotor factor and all
625 significant GLM coefficients (GFAP, PV, plus LTP: r^2 = 0.7974, p = 0.0116; Fig.
626 5H), as well as sensorimotor factor and univariate neurobiological measures
627 (GFAP: r = 0.6840, p = 0.0099; Fig. 5I, PV: r = 0.6548, p = 0.0151; Fig. 5J).
628 Strikingly, we found a quadratic relationship between synaptic plasticity
629 effects and measures of cognitive impairment. Poor performance on the working
630 memory test was observed in rats that presented too low or too high values of
631 HPC-PFC LTP, suggesting a U-shaped relationship between LTP and cognitive
632 performance (Fig. 5K-L). We observed this quadratic relationship using both the
633 cognitive factor (gaussian GLM, LTP coefficient = 1.22, p = 0.0162; Fig. 5K) and
634 raw error values from the radial maze test using a quasi-Poisson GLM (p =
635 0.00843; Fig. 5L).
636 Taken together, our analysis demonstrates that both neuroinflammation
637 and synaptic plasticity alterations may underlie the behavioral effects of ELS, with
638 neuroinflammation being more associated with the sensorimotor dimension and
639 LTP with the cognitive dimension.

640

641 **ELS animals present epileptiform-like activity when adults**

642 Given the results above indicating ELS impacts on specific behavioral
643 demands, large-scale networks, and HPC-PFC functional connectivity, we
644 decided to investigate ELS-related dysfunctions in circuit dynamics across
645 different brain-behavioral states using chronic electrophysiology recordings. We
646 hypothesized that HPC-PFC communication is altered in ELS animals, showing
647 aberrant oscillatory patterns in the circuit. First, we classified LFP epochs into
648 active wake (ACT), non-REM (NREM) sleep, rapid eye movement sleep (REM),
649 and quiet wake (QWK; Fig. 6A-D). No CTRL *vs.* ELS differences were found in
650 sleep architecture, according to the mean consecutive duration of each state,
651 percentage of time awake, number of persistent episodes in each state (Two-way
652 RM ANOVA, $F_{(1,13)} = 0.6500$, $p > 0.4346$; Fig. 6E-G), and percentage of time in
653 each state (Two-way RM ANOVA, $F_{(1,13)} = 0.5425$, $p > 0.4745$; Fig. 6H).

654 We also examined if ELS animals displayed ictal activity during recordings.
655 We found that 44.45% of the ELS animals presented electrographic discharges
656 similar to spike-wave discharges (SWD) or rhythmical spiking (Fig. 6H-I). The
657 mean duration of the electrographical ictal activity was 6.614±0.1416 s
658 (coefficient of variation: 4.281%) and the total duration was 38.98±11.25 min
659 (coefficient of variation: 57.70%). SWDs occurred mainly during NREM sleep
660 and less often in QWK and ACT but rarely occurred during REM epochs (Fig 6J-
661 M). The SWDs were not found in the CTRL rats, indicating that ELS induces an
662 epileptogenic process.

663

664 **Increased HPC theta power during behavioral activity in ELS animals**

665 We initially concentrated our investigation on the ACT behavioral state to
666 associate oscillatory patterns with the behavioral abnormalities observed. We
667 found that ELS animals presented a higher theta power during ACT states in the
668 HPC (*t*-test, $t_{(13)} = 2.259$, $p = 0.0417$; Fig. 7A-D), but not in the PFC (*t*-test, $t_{(13)} =$
669 0.2636, $p = 0.7961$; Fig. 7B). This increased theta activity is more prominent
670 during the first periods of recording and exploration of the new environment
671 (linear mixed-effects model, $t = 2.10$, $p = 0.055$; Uncorrected *t*-tests for period
672 comparison: $t_{(13)} = 2.145$, 2.367, and 2.319, $p = 0.051$, 0.034, and 0.037 for
673 periods 1, 2, and 3, respectively; Fig. 7E). To further explore whether theta power

increase reflects a true oscillation and is not due to alterations in the aperiodic components of the PSD, we also performed a PSD parametrization to separate the theta oscillation (Fig. 7F). We found an increase in the theta oscillatory activity in ELS animals during ACT states, indicating an actual oscillatory effect (Mann-Whitney, U = 7, n = (6,9), p = 0.0176; Fig. 7G-H). Hippocampal theta is well known to occur during periods of locomotor activity, e.g., postural changes, head movements, and rearing (Buzsáki and Moser, 2013) representing a possible confounder. To control for this, we co-examined HPC theta power and EMG distributions during active states in CTRL *vs.* ELS rats (Fig. 7I). Indeed, theta oscillatory increase in ELS animals did not appear to be related to more movement, as we did not observe a significant association between EMG and theta power. In contrast, we found higher theta power in ELS animals even at low levels of EMG activity (Fig. 7I).

ELS promotes abnormal gamma coordination in the PFC during behavioral activity

Considering the extensively documented involvement of PFC gamma activity in cognitive and sensory processes, as well as its alterations observed in animal models of neurodevelopmental and psychiatric disorders such as ASD and schizophrenia (Rojas and Wilson, 2014; Sigurdsson, 2016), we investigated the possible effects of ELS on PFC gamma activity during active states. ELS animals showed a reduced theta-gamma amplitude correlation during ACT states (t-test, $t_{(13)}$ = 2.851, p = 0.0136; Fig. 8A-C), indicating that high-gamma activity is less coordinated, despite the increase in theta power. Interestingly, there were no increases in both low or high-gamma power (low-gamma: Mann-Whitney, U = 16, n = (6,9), p = 0.2238; high-gamma: Mann-Whitney, U = 24, n = (6,9), p = 0.7756; Fig. 8D). Amplitude correlation is an indicator of large-scale cortical interactions that govern cognition (Siegel et al., 2012). Thus, the lower theta-high gamma correlations found here may be related to the cognitive disruptions caused by ELS.

Next, we found a reduction in the PFC spectral exponent in ELS animals assessed by aperiodic PFC activity during ACT state (note the flatter spectra of ELS in Fig. 8E), distribution of the aperiodic component (exponent and offset, Fig 8F), and comparison in exponent parameter between groups (t-test, $t_{(13)}$ =

2.010, p = 0.0656; Fig. 8G). Reductions of the spectral exponent have been discussed to indicate increased excitation/inhibition imbalance (Gao et al., 2017). This abnormal gamma dynamics in the ELS indicates a less coordinated oscillatory activity, which may reflect impaired limbic-cortical or cortico-cortical interactions that underlie cognitive dysfunctions.

ELS impairs HPC-PFC coherence during REM sleep

HPC-PFC connectivity and information flow during REM sleep is essential for memory consolidation (Lesting et al., 2013). Because we found cognitive impairments in ELS animals, we investigated HPC-PFC interactions during REM. First, we observed that the theta power in the PFC and HPC during REM is not different between groups (PFC: t-test, $t_{(13)}$ = 1.320, p = 0.2096; HPC: t-test, $t_{(13)}$ = 0.3557, p = 0.7278; Fig. 9A-B). However, we found that ELS rats show reduced HPC-PFC connectivity in the theta band, measured by spectral coherence during REM sleep (t-test, $t_{(13)}$ = 2.183, p = 0.0480; Fig. 9C-D). This difference occurs throughout the entire recording, as observed by the comparisons for all 6-hour periods (linear mixed-effects model, t = -2.27, p = 0.0408; Fig. 9D, right). We further confirmed this difference by analyzing the cross-correlation and cross-spectrum power of the HPC-PFC LFP during REM (Fig. 9E-G). Cross-correlation analysis reveals a clear directionality between signals from the HPC to the PFC in both groups that happens markedly at a specific lag (-80 to -20 ms; Fig. 9E), in which ELS rats present the most profound decrease in the correlation peak (t-test, $t_{(13)}$ = 2.533, p = 0.0250; Fig. 9F-G).

We noticed from inspecting the theta coherence changes between ACT and REM – the two states with the strongest theta coherence – that all CTRL animals exhibited greater theta coherence during REM (paired t-test, $t_{(5)}$ = 8.023, p = 0.0005; Fig. 9H), while in the ELS group, part of the animals did not present such an increase (paired t-test, $t_{(8)}$ = 1.924, p = 0.09; Fig. 9H). This dynamic is further illustrated by observing the coherence changes across REM, QWK, and ACT states. While most CTRL rats present an inclined decrease from REM to QWK and a slight increase from QWK to ACT, ELS rats display a flatter curve (Fig. 9I). By quantifying the homogeneity of the distributions of average theta coherence values across states with entropy, we found a significantly higher entropy (more homogeneous) in ELS than CTRL (paired t-test, $t_{(13)}$ = 2.695, p =

742 0.0184; Fig. 9J). These results indicate that ELS promotes impairment in HPC-
743 PFC connectivity during REM sleep and in the regulation of state-dependent
744 dynamics.
745
746 **ELS rats display REM-like oscillatory dynamics during active behavior**
747 The distinct neural processes occurring at each state during the
748 sleep/wake cycle are crucial for brain homeostasis**.** After we noticed that ELS
749 animals show less distinction of some electrophysiological activities between
750 brain states, particularly REM and ACT, we decided to carry out an in-depth
751 characterization of the long-term effects of ELS on HPC-PFC state-dependent
752 oscillatory dynamics across the sleep-wake cycle. For that, we used the state
753 map framework, which employs two spectral power ratios, allowing consistent
754 characterization of all major brain states and revealing a dynamic global structure
755 produced by the collective activity of forebrain structures (Dzirasa et al., 2006;
756 Gervasoni et al., 2004). First, we verified that the state maps reflected other brain
757 and muscle activities that were not directly used for the map construction, such
758 as the concentrated distribution of the PFC delta power during NREM, of the HPC
759 theta/delta ratios in REM, of the EMG power in awake states, and of HPC-PFC
760 theta coherence in both REM and awake states (Fig. 10A). Thus, as expected,
761 our state maps presented three distinct clusters that precisely located REM,
762 NREM, and ACT epochs (Fig. 10B).
763 Using this approach, a previous study reported an overlap between awake
764 and REM states in a hyperdopaminergic mouse model (Dzirasa et al., 2006).
765 Because we found ELS-related functional changes specifically during ACT and
766 REM, we sought to investigate the convergence between these two states.
767 Remarkably, we also found that ELS rats showed a significant similarity between
768 the REM and ACT states (Fig. 10B). While in CTRL rats the distributions of
769 Euclidean distances were larger, homogeneous, and symmetrical (Fig. 10C),
770 ELS rats presented highly variable patterns across animals, most of which with
771 skewed distributions concentrated at shorter distances (Fig. 10C). Indeed, the
772 Euclidean distance was significantly reduced in ELS (*t*-test, $t_{(13)} = 2.326$, $p =$
773 0.0369; Fig. 10D), suggesting that the spectral features of REM and ACT are
774 more similar in ELS animals.

775 Interestingly, we observed that this difference in states similarity was
776 stronger in the initial 12 hours of recording, which corresponds to the periods of
777 habituation to the novel environment (*t*-test, for periods 1-2: $t_{(13)} = 2.45$, $p = 0.029$;
778 for periods 3-4: $t_{(13)} = 0.9409$, $p = 0.3638$; Fig. 10E).
779 To further demonstrate the higher similarity between REM and ACT states
780 in ELS animals, we used machine learning algorithms in an attempt to separate
781 these brain states through a *brute-force* approach. We observed that the two
782 algorithms tested had a worse discrimination performance in the ELS rats, as
783 verified by the smaller AUC-ROC (*t*-test, for SVM: $t_{(198)} = 99.59$, $p < 0.0001$; for
784 random forest: $t_{(198)} = 107.6$, $p < 0.0001$; Fig. 10F). This worse discriminative
785 performance also arises when using random forest algorithm (which presents the
786 best discriminative performance) on the original whole-spectrum high-
787 dimensional variables (*t*-test, for PFC power: $t_{(198)} = 21.34$, $p < 0.0001$; for HPC
788 power: $t_{(198)} = 58.78$, $p < 0.0001$; for coherence: $t_{(198)} = 80.82$, $p < 0.0001$; for all
789 the spectral estimates combined: $t_{(198)} = 39.23$, $p < 0.0001$; Fig. 10G). This lack
790 of discriminative performance once again corroborates spectral similarities
791 between REM and ACT states in ELS rats.
792
793 **ELS rats present behavioral and neurochemical sensitivity to dopaminergic**
794 **activation**
795 Similar to our findings on ELS, REM-like neural oscillations during
796 wakefulness were described in pharmacological and genetic animal models of
797 hyperdopaminergia (Dzirasa et al., 2006). Particularly, hyperdopaminergia has
798 also been implicated in experimental models of schizophrenia as underlying
799 impairments of sensorimotor gating and working memory deficits (Grace, 2016),
800 whereas dopamine is known to optimally regulate synaptic plasticity (Otani et al.,
801 2015). Taken together, these convergent findings suggest altered dopaminergic
802 transmission as a plausible candidate to underlie some of the major effects of
803 ELS. To investigate whether ELS promotes alterations in dopaminergic
804 transmission or sensitivity,, we conducted a final experiment assessing the
805 behavioral and neurochemical sensitivity to dopaminergic activation using
806 apomorphine (unspecific dopaminergic agonist). We examined behavioral
807 sensitivity by comparing the locomotion produced by apomorphine in the open
808 field (Fig. 11A). Our data demonstrate that apomorphine produces a higher

809 increase in locomotion in ELS rats when compared to CTRL across time blocks
810 (Two-way RM ANOVA, treatment effect: $F_{(1,27)} = 4.260$, $p = 0.0487$, Sidak's *post-*
811 *hoc:* 5 min $p = 0.0376$; Fig. 11B) or between average normalized distances
812 (Mann-Whitney, *n(CTRL, ELS)* = 14/15, $U = 32$, $p = 0.0009$; Fig. 11B inset).
813 Immediately after the behavioral test, we collected samples of NAc, PFC,
814 and HPC to quantify neurotransmitters. The NAc was included in this analysis
815 because it is highly implicated in dopamine sensitivity and exploratory behavior
816 (Salomone et al., 2012). Our data demonstrate that apomorphine reduces
817 dopamine in the NAc of ELS rats, with no effects on dopamine turnover, as
818 measured by DOPAC/DA ratio (Sidak's multiple correction procedure, $t_{(12)} =$
819 3.656, $p = 0.0033$; Fig. 11C). Still, a GLM model implicated NAc dopamine
820 turnover as a significant predictor of apomorphine-induced hyperlocomotion
821 (*coefficient* = -0.7108, $p = 0.00297$; Fig. 11D). Consistently, apomorphine is
822 known to reduce endogenous DA release and DA metabolism in rodents and
823 humans (De La Fuente-Fernández et al., 2001; Ozaki et al., 1989). We also
824 observed a reduction in dopamine turnover in the HPC of ELS rats (Sidak's
825 multiple correction procedure, $U = 9$, $p = 0.0164$; Fig. 11E) but no significant
826 effects in the PFC.
827 Interestingly, we found that the HPC of ELS rats shows a higher Glu
828 content and higher Glu/GABA ratio than CTRL animals following apomorphine
829 injection (Sidak's multiple correction procedure, Glu: $t_{(15)} = 2.566$, $p = 0.0215$;
830 Glu/GABA: $U = 9$, $p = 0.0079$; Fig. 12F) indicating possible disturbances in the
831 excitation/inhibition balance.
832
833 **HPC-PFC oscillatory dynamics discriminate ELS individuals**
834 After identifying the relevance of specific electrophysiological variables
835 throughout the study, we sought to investigate if collective patterns of the
836 electrophysiological covariates across individuals could assemble a
837 multidimensional oscillatory signature that distinguishes the ELS subjects. Based
838 on relevance, particularity, and state specificity, for this investigation, we chose:
839 (1) HPC theta power (Fig. 7H), (2) theta coherence entropy (Fig. 9J), (3) PFC
840 exponent (Fig. 8G), (4) PFC theta-gamma correlation (Fig. 8C), (5) theta
841 coherence (Fig. 9D), and (6) state map distance (Fig. 10D). By performing PCA,
842 we observed that the first two principal components completely discriminated

843 ELS from CTRL animals (Fig. 12A). This discrimination was further confirmed by
844 fitting a linear discriminant classifier (traces on Fig. 12A) that achieved a 100%
845 accuracy using the entire dataset and 80% accuracy on leave-one-out cross-
846 validation.

847 Furthermore, unsupervised clustering almost completely discriminated
848 ELS from CTRL rats dividing all the animals into two major clusters: a
849 predominantly ELS cluster (81.82% of ELS animals) and a complete CTRL
850 cluster (100% of CTRL animals; Fig. 12B). The hierarchical clustering approach
851 evidenced a progression of ELS-related oscillatory alterations, with a subcluster
852 presenting an overlap between ELS and CTRL but the other with a more
853 pronounced abnormal spectral fingerprint (Fig. 12B). In addition, the values of
854 each variable are distinct in each group, which demonstrates that the
855 electrophysiological variables used here are jointly affected by ELS at the
856 functional level. Finally, we show that all the single electrophysiological variables
857 have a high discriminative value (AUC > 0.7) (Fig. 12D), yet, their multivariate
858 linear combination represented by PC1 scores (Fig. 12A) has the best
859 classification performance with an AUC of 1.

860

861 **Discussion**

862 Here we showed that although ELS does not induce significant neuronal
863 death, it leads to long-term cognitive impairments and behavioral abnormalities.
864 These effects are correlated with neuronal inflammation, hypersensitive
865 dopaminergic neurotransmission, and aberrant HPC-PFC synaptic plasticity. We
866 also found that ELS rats exhibit brain state-dependent alterations – particularly
867 during active behavior and REM sleep – characterized by increased theta power
868 and impaired coordination of local and long-range activity. In addition, ELS
869 presents an abnormal oscillatory state during active behavior oddly similar to
870 REM sleep. Finally, the collective pattern of oscillatory alterations accurately
871 distinguishes ELS from control animals.

872

873 **Common pathophysiological mechanisms underlying ELS consequences**
874 **and psychiatric-like impairments**

875 Remarkably, the behavioral alterations found here are well-established
876 translational features of neurodevelopmental disorders and psychiatric disorders

877 related to epilepsy. Studies usually describe increased locomotion (Kubová and
878 Mareš, 2013) and working memory deficits (Tsai et al., 2012) as consequences
879 of ELS. In addition, we also found a reduced PPI, which is less studied but
880 represents a well-established correlate of positive symptoms in clinical psychosis
881 and sensorimotor alterations of ASD (Cheng et al., 2018; Turetsky et al., 2007;
882 Ziermans et al., 2011). Here, we demonstrated a multivariate *sensorimotor factor*
883 comprising a collection of behaviors frequently reported in animal models of
884 schizophrenia, ADHD, and ASD (Ey et al., 2011; Regan et al., 2022; Sigurdsson,
885 2016). Furthermore, we demonstrated a *cognitive factor* mainly representing
886 working memory deficits, a hallmark in several neurodevelopmental models and
887 psychiatric comorbidities, particularly schizophrenia (Cope et al., 2016).
888 Importantly, the two factors were uncorrelated, but both resulted from ELS. This
889 lack of association between cognitive and sensorimotor impairments suggests
890 two neurobiological substrates, which are confirmed by our multivariate analysis,
891 indicating the association of LTP to cognitive deficits and neuroinflammation to
892 sensorimotor alterations.

893 Surprisingly, we found that cognitive impairment was associated with an
894 abnormally increased susceptibility of HPC-PFC circuits to undergo LTP. This
895 appears to be in contrast with previous studies, which reported reduced
896 hippocampal LTP and cognitive deficits after ELS (Chang et al., 2003; O'Leary et
897 al., 2016). However, no hyperexcitability or spontaneous seizures were described
898 in these studies (O'Leary et al., 2016). In turn, Notenboom et al. (2010) used an
899 animal model of febrile ELS and demonstrated increased LTP in HPC slices
900 related to the reduction of seizure threshold, hyperexcitability, and spontaneous
901 seizures later in life (i.e., epileptogenesis) (Dubé et al., 2006a; Dube et al., 2000).
902 Indeed, paroxysmal activity has been shown to acutely increase synaptic efficacy
903 and hippocampal LTP, thereby reducing the threshold for seizure induction (Ben-
904 Ari & Gho, 1988; Minamiura et al., 1996). In this context, the enhanced LTP
905 observed in our data indicates a relationship with epileptogenesis, which concurs
906 with the epileptiform discharges observed in ELS rats and the increases observed
907 in the hippocampal Glu/GABA ratio.

908 We describe an inverted-U relationship between LTP and working
909 memory, suggesting an optimal level of LTP susceptibility is required for
910 adequate working memory performance. Aberrant synaptic plasticity could be a

common mechanism between cognitive deficits and epileptogenesis induced by ELS. Hyperexcitable HPC-PFC circuits could facilitate the spread of epileptiform activity and promote alterations in synaptic saturation and excitatory/inhibitory balance, ultimately leading to cognitive deficits. In this sense, the abnormally increased LTP could impair sensory processes during working memory and explain the poor performance we observed in ELS rats. In a neural network with aberrantly enhanced LTP, synaptic plasticity could be biased toward potentiation, resulting in a lower ability to retain information or adapt to the environment (Navakkode et al., 2022). This rationale is supported by several genetic studies, including on risk genes for neuropsychiatric disorders and autism that described relationships between enhanced LTP and impaired learning (Garcia-Alvarez et al., 2015; Meng et al., 2002; Nuytens et al., 2013; Yokoi et al., 2015). Interestingly, hyperdopaminergic signaling enhanced HPC-PFC LTP dose-dependently following an "inverted-U" function, where too high or too low dopamine levels disrupted LTP induction, indicating that altered DA neurotransmission could underlie the LTP abnormalities in ELS rats (Goto and Grace, 2006; Otani et al., 2015).

We also report an increase in GFAP expression in ELS animals. Inflammatory processes initiated by a brain insult could lead to functional impairments and, ultimately, psychiatric symptoms (Vezzani et al., 2013). In ELS models, long-term glial activation has been related to behavioral impairments and epileptogenesis (De Oliveira et al., 2008b), while treatment with inflammatory inhibitors resulted in reductions of GFAP and cognitive impairments (Abraham et al., 2012; Somera-Molina et al., 2007). High levels of pro-inflammatory substances and neuroinflammation have been documented in animal models and patients with schizophrenia and ASD (Prata et al., 2017; Vezzani et al., 2013). Noteworthy, the HPC of patients with temporal lobe epilepsy (TLE) and interictal psychosis present greater GFAP and microglia activation than TLE patients without psychosis (Kandratavicius et al., 2015). Additionally, GFAP is elevated in the frontal cortex of autistic subjects (Laurence and Fatemi, 2005). These findings are in accordance with clinical and preclinical biomarkers bridging psychosis and ASD to dopaminergic disturbances resulting from ELS.

In adult SE studies, behavioral abnormalities and cognitive deficits have been positively correlated to neuronal loss and spontaneous seizure frequency

(Wolf et al., 2016). It is suggested that the etiological mechanisms of neuropsychiatric-related alterations and epileptic excitability spread progressively over time. Indeed, the behavioral impairments in ELS models tend to be more subtle than in animal models of TLE or hyperdopaminergia. It is possible that the observed alterations in neuroinflammation, neuronal dynamics, and neurochemistry represent initial epileptogenic pathological mechanisms that could progress to spontaneous seizures, progressive neuronal loss, and more intense behavioral manifestations (Dubé et al., 2006b; Kubová and Mareš, 2013).

Dysfunctional patterns of HPC-PFC oscillatory dynamics

Our results demonstrate a locomotion-unrelated increase in HPC theta power during active behavior in ELS animals. Theta oscillations underlie various cognitive processes and are believed to serve as a temporal organizer for multiple functions, such as sensorimotor integration (Buzsáki and Moser, 2013). However, increases in HPC theta power are also observed in hyperdopaminergic-like states, such as following the administration of ketamine or a dopaminergic agonist (Caixeta et al., 2013; Thörn et al., 2022). Increases in theta power are reported in most studies in patients with schizophrenia (Newson and Thiagarajan, 2019) and have been correlated with poor cognitive performance (Curic et al., 2021). Thus, stronger HPC theta power does not necessarily reflect an optimal cognitive state. In fact, abnormal and increased theta power has been described as a consequence of ELS in different models and related to cognitive impairment (Kleen et al., 2011; Velasquez et al., 2023).

Here we observed lower theta-gamma correlations in the PFC of ELS animals, suggesting a disconnection between theta power and local coordination of PFC activity. Similarly, the prolonged febrile model of ELS also resulted in a decreased coordination of gamma activity in the hippocampal circuits (Kloc et al., 2023). In addition, we also observed a flatter PFC power spectrum in ELS animals compared to the normal tilt of CTRL, which has been discussed to indicate excitation/inhibition imbalance (Gao et al., 2017). These findings occurring during active behavior could explain the cognitive-behavioral alterations we observed, at least to some extent.

Desynchronization between limbic-frontal circuits is also reflected by reduced theta coherence during REM. Genetic and neurodevelopmental models

979 of cognitive disorders exhibit a decrease in HPC-PFC theta synchrony correlated
980 with poor spatial working memory performance and anxiety behaviors (Cunniff et
981 al., 2020; Sigurdsson, 2016; Sigurdsson and Duvarci, 2016). Interestingly,
982 increased HPC-PFC theta coherence was described in a model of repetitive ELS
983 (Holmes et al., 2015; Mouchati et al., 2019). Specifically, this enhanced
984 coherence was observed during cognitive performance and associated with a
985 mechanism of neuronal compensation (Kleen et al., 2011; Niedecker et al., 2021).
986 However, during REM sleep, these studies reported a decreased coherence and
987 phase-locking value, indicating different synchronization dynamics depending on
988 the brain state (Niedecker et al., 2021). Here, we observed impaired theta
989 coherence only during REM sleep, which is the brain state with the expected
990 highest coherence values, indicating that ELS animals could not reach or
991 maintain this connectivity at the same maximum capacity as CTRL animals. The
992 results from oscillatory dynamics in the HPC-PFC circuit indicate persistent state-
993 dependent abnormalities in the temporal organization and interaction of local
994 circuits that can contribute to long-term behavioral alterations and cognitive
995 deficits. Further exploration should investigate HPC-PFC coordination during
996 specific cognitive demands, such as working memory tasks, which we have
997 shown to be impaired following ELS.

998 Our results also demonstrated that during ACT behavior, frontal-limbic
999 oscillatory dynamics of ELS rats are unusually similar to REM sleep. Importantly,
1000 this finding could not be explained by altered locomotion or sleep architecture.
1001 This aberrant active state was more pronounced in the initial 12 h of recording,
1002 corresponding to the habituation to the novel environment. Dzirasa et al. (2006)
1003 found similar results when recording hyperdopaminergic mice. The authors
1004 described a REM-like awake state in DAT-KO mice and wild-type mice injected
1005 with amphetamine. Similar to our results, the hyperdopaminergic wake state was
1006 marked by a significant increase in hippocampal theta oscillations. Additionally,
1007 treatment with antipsychotics reduced these REM-like hippocampal oscillations
1008 (Dzirasa et al., 2006). Our similar findings on a developmental model resulting in
1009 a psychotic-like phenotype support the relevance of intraindividual REM-wake
1010 similarity as a neural mechanism of psychosis. These results also advance
1011 previous studies, suggesting a shared involvement of dopamine in the impaired
1012 regulation of state-dependent global network dynamics in animal models of

1013 psychosis and epilepsy. Also interestingly, it is speculated that REM-wake
1014 similarity may represent a neural correlate of oneiric intrusion onto awake
1015 consciousness (Dzirasa et al., 2006), which, in the clinical context, could underlie
1016 potential phenomenological manifestations of sensorimotor disturbances of
1017 neurodevelopmental or psychiatric disorders.

1018 In support of these dopaminergic alterations, we showed that ELS
1019 promotes apomorphine hypersensitivity and alterations in dopamine
1020 neurotransmission. Apomorphine sensitivity has been associated with reduced
1021 PPI, hyperlocomotion, and increased NAc dopamine release (Ellenbroek and
1022 Cools, 2002). Corroborating our data, neonatal SE promotes amphetamine
1023 sensitization and affects both dopaminergic and glutamatergic levels in
1024 prefrontal-striatal circuits (Lin et al., 2009). Importantly, alterations in dopamine
1025 signaling have been implicated in schizophrenia, ASD, and ADHD (Grace, 2016;
1026 Kollins and Adcock, 2014; Kosillo and Bateup, 2021). These results point to
1027 enhanced dopaminergic neurotransmission as a potential mechanism underlying
1028 the functional abnormalities observed in ELS rats.

1029 Importantly, the observed alterations in mesolimbic dopaminergic activity,
1030 coupled with increased neuroinflammation in thalamic nuclei, imply broader-scale
1031 brain alterations beyond the confines of the HPC-PFC circuitry. While our findings
1032 on synaptic plasticity and oscillatory patterns suggest a robust connection
1033 between behavioral manifestations and dysfunctional communication within the
1034 HPC-PFC circuit, it is plausible that SE induces dysfunction on a broader network
1035 scale. Notably, theta oscillation and state-map examination may represent larger-
1036 scale limbic-cortical dynamics that extend beyond the HPC-PFC circuit.
1037 Consolidated evidence underscores the concept that cognitive and executive
1038 functions arise from the coordinated activity of large-scale networks (Ulhaas and
1039 Singer, 2012). In this context, the disruption of functional large-scale networks
1040 may play a causal role in neuropsychiatric disorders and account for several
1041 specific dysfunctions associated with these conditions (Ulhaas and Singer, 2012).

1042 The aim of our work was to establish a comprehensive framework of ELS
1043 behavioral and neurobiological outcomes to provide a foundation for future
1044 research delving into target interventions. In this context, we acknowledge that
1045 most of our findings are correlational, therefore, studies investigating causal
1046 manipulations will be paramount for establishing cause-and-effect links and

1047 understanding the chain of biological events that happen in the aftermath of ELS
1048 leading to behavioral and cognitive deficits. Still, our initial data-driven approach
1049 was able to reveal nuanced relationships, such as multivariate associations and
1050 non-linear relationships, that could not have been revealed through simple
1051 univariate analysis or causally perturbing single factors at first. Based on our
1052 findings and the supporting literature, particular targets for the following
1053 investigations stand out. We speculate that facilitating HPC-PFC LTP
1054 susceptibility could boost working memory performance in CTRL animals while
1055 blocking it could improve it for ELS. Also, we hypothesize that long-term inhibition
1056 of astrogliosis and neuroinflammation after ELS could attenuate subsequent
1057 sensorimotor impairments. Finally, we conjecture that aberrant plasticity and
1058 abnormal network dynamics could be normalized by dopaminergic inactivation in
1059 ELS animals. Thus, further studies performing causal manipulations will help us
1060 understand the mechanisms of ELS and bridge our findings with the development
1061 of new treatments for neurodevelopmental disorders.

1062 In conclusion, we describe a comprehensive set of behavioral and
1063 neurobiological alterations following ELS that represent common patterns of
1064 dysfunctional circuit dynamics between developmental brain disturbances and
1065 multiple comorbidities associated. Although further studies should investigate
1066 causal links between neurobiological and behavioral alterations, our findings
1067 integrate a prominent theory about the pathogenesis of psychiatric symptoms that
1068 links stressful insults during development to increased HPC excitability, which
1069 would culminate in the hyperactivation of the mesolimbic system, resulting in
1070 behavioral dysfunctions (Gomes et al., 2020). Our results add depth to this theory
1071 by finding relationships among (1) neurodevelopmental insult, (2)
1072 neuroinflammation, (3) hyperexcitable HPC, (4) increased DA drive, (5) disrupted
1073 information flow in limbic-frontal circuits, and (6) psychiatric-relevant behaviors.
1074 Given the common pathophysiological and behavioral traits linking
1075 epileptogenesis and behavioral-cognitive comorbidities, we emphasize the
1076 experimental model's validity to investigate the neurobiological mechanisms of
1077 how an injury during development can lead to neuropsychiatric symptoms. Our
1078 study also demonstrates the potential of a multilevel strategy combining
1079 electrophysiology, behavior, immunohistochemistry, and neurochemistry in

1080 revealing integrated multidimensional mechanisms linking developmental
1081 impacts to epilepsy, cognition, and psychiatric symptoms.
1082

1083 **References**

1084 Abraham J, Fox PD, Condello C, Bartolini A, Koh S. 2012. Minocycline attenuates
1085 microglia activation and blocks the long-term epileptogenic effects of early-
1086 life seizures. *Neurobiol Dis* **46**:425–430. doi:10.1016/j.nbd.2012.02.006

1087 Baram TZ, Eghbal-Ahmadi M, Bender RA. 2002. Is neuronal death required for
1088 seizure-induced epileptogenesis in the immature brain?Progress in Brain
1089 Research. Elsevier. pp. 365–375. doi:10.1016/S0079-6123(02)35033-7

1090 Barr DJ, Levy R, Scheepers C, Tily HJ. 2013. Random effects structure for
1091 confirmatory hypothesis testing: Keep it maximal. *J Mem Lang* **68**:255–278.
1092 doi:10.1016/j.jml.2012.11.001

1093 Barry J, Mahoney J, Holmes G. 2020. Coordination of Hippocampal Theta and
1094 Gamma Oscillations Relative to Spatial Active Avoidance Reflects Cognitive
1095 Outcome After Febrile Status Epilepticus. *Behavioral Neuroscience* **134**:562–
1096 576. doi:10.1037/bne0000388.supp

1097 Ben-Ari Y and, Gho M. 1988. LONG-LASTING MODIFICATION OF THE
1098 SYNAPTIC PROPERTIES OF RAT CA3 HIPPOCAMPAL NEURONES
1099 INDUCED BY KAINIC ACID, Journal of Physiology.

1100 Brunquell PJ, Glennon CM, DiMario FJ, Lerer T, Eisenfeld L. 2002. Prediction of
1101 outcome based on clinical seizure type in newborn infants. *Journal of*
1102 *Pediatrics* **140**:707–712. doi:10.1067/mpd.2002.124773

1103 Bueno-Junior LS, Peixoto-Santos JE, Ruggiero RN, Ávila MAV, Marques DB,
1104 Lopes-Aguiar C, Leite JP. 2018. Interaction between hippocampal-prefrontal
1105 plasticity and thalamic-prefrontal activity. *Sci Rep* **8**. doi:10.1038/s41598-
1106 018-19540-6

1107 Bueno-Junior LS, Ruggiero RN, Rossignoli MT, Del Bel EA, Leite JP, Uchitel OD.
1108 2017. Acetazolamide potentiates the afferent drive to prefrontal cortex
1109 in vivo. *Physiol Rep* **5**. doi:10.14814/phy2.13066

1110 Buzsáki G, Moser EI. 2013. Memory, navigation and theta rhythm in the
1111 hippocampal-entorhinal system. *Nat Neurosci*. doi:10.1038/nn.3304

1112 Caixeta F V., Cornélio AM, Scheffer-Teixeira R, Ribeiro S, Tort ABL. 2013.
1113 Ketamine alters oscillatory coupling in the hippocampus. *Sci Rep* **3**.
1114 doi:10.1038/srep02348

1115 Castelhano ASS, Cassane G dos ST, Scorza FA, Cysneiros RM. 2013. Altered
1116 anxiety-related and abnormal social behaviors in rats exposed to early life
1117 seizures. *Front Behav Neurosci*. doi:10.3389/fnbeh.2013.00036

1118 Castro-Neto EF de, Cunha RH da, Silveira DX da, Yonamine M, Gouveia TLF,
1119 Cavalheiro EA, Amado D, Naffah-Mazzacoratti M da G. 2013. Changes in
1120 aminoacidergic and monoaminergic neurotransmission in the hippocampus
1121 and amygdala of rats after ayahuasca ingestion. *World J Biol Chem* **4**:141.
1122 doi:10.4331/wjbc.v4.i4.141

1123 Chang Y-C, Huang A-M, Kuo Y-M, Wang S-T, Chang Y-Y, Huang C-C. 2003.
1124 Febrile Seizures Impair Memory and cAMP Response-Element Binding
1125 Protein Activation.

1126 Cheng CH, Chan PYS, Hsu SC, Liu CY. 2018. Meta-analysis of sensorimotor
1127 gating in patients with autism spectrum disorders. *Psychiatry Res* **262**:413–
1128 419. doi:10.1016/j.psychres.2017.09.016

1129 Cope ZA, Powell SB, Young JW. 2016. Modeling neurodevelopmental cognitive
1130 deficits in tasks with cross-species translational validity. *Genes Brain Behav*.
1131 doi:10.1111/gbb.12268

1132 Cunniff MM, Markenscoff-Papadimitriou E, Ostrowski J, Rubenstein JLR, Sohal
1133 VS. 2020. Altered hippocampal-prefrontal communication during anxiety-
1134 related avoidance in mice deficient for the autism-associated gene pogz. *Elife*
1135 **9**:1–27. doi:10.7554/eLife.54835

1136 Curic S, Andreou C, Nolte G, Steinmann S, Thiebes S, Polomac N, Haaf M, Rauh
1137 J, Leicht G, Mulert C. 2021. Ketamine Alters Functional Gamma and Theta
1138 Resting-State Connectivity in Healthy Humans: Implications for
1139 Schizophrenia Treatment Targeting the Glutamate System. *Front Psychiatry*
1140 **12**. doi:10.3389/fpsyt.2021.671007

1141 De La Fuente-Fernández R, Lim AS, Sossi V, Holden JE, Calne DB, Ruth TJ,
1142 Stoessl AJ. 2001. Apomorphine-Induced Changes in Synaptic Dopamine
1143 Levels: Positron Emission Tomography Evidence for Presynaptic Inhibition.

1144 De Oliveira DL, Fischer A, Jorge RS, Da Silva MC, Leite M, Gonçalves CA,
1145 Quillfeldt JA, Souza DO, E Souza TM, Wofchuk S. 2008a. Effects of early-life
1146 LiCl-Pilocarpine-induced status epilepticus on memory and anxiety in adult
1147 rats are associated with mossy fiber sprouting and elevated CSF S100B
1148 protein. *Epilepsia* **49**:842–852. doi:10.1111/j.1528-1167.2007.01484.x

1149 De Oliveira DL, Fischer A, Jorge RS, Da Silva MC, Leite M, Gonçalves CA,
1150 Quillfeldt JA, Souza DO, E Souza TM, Wofchuk S. 2008b. Effects of early-life
1151 LiCl-Pilocarpine-induced status epilepticus on memory and anxiety in adult
1152 rats are associated with mossy fiber sprouting and elevated CSF S100B
1153 protein. *Epilepsia* **49**:842–852. doi:10.1111/j.1528-1167.2007.01484.x

1154 Donoghue T, Haller M, Peterson EJ, Varma P, Sebastian P, Gao R, Noto T, Lara
1155 AH, Wallis JD, Knight RT, Shestyuk A, Voytek B. 2020. Parameterizing neural
1156 power spectra into periodic and aperiodic components. *Nat Neurosci*
1157 **23**:1655–1665. doi:10.1038/s41593-020-00744-x

1158 Dreier JW, Pedersen CB, Cotsapas C, Christensen J. 2019. Childhood seizures
1159 and risk of psychiatric disorders in adolescence and early adulthood: a
1160 Danish nationwide cohort study. *Lancet Child Adolesc Health* **3**:99–108.
1161 doi:10.1016/S2352-4642(18)30351-1

1162 Drysdale AT, Grosenick L, Downar J, Dunlop K, Mansouri F, Meng Y, Fetcho RN,
1163 Zebley B, Oathes DJ, Etkin A, Schatzberg AF, Sudheimer K, Keller J,
1164 Mayberg HS, Gunning FM, Alexopoulos GS, Fox MD, Pascual-Leone A, Voss
1165 HU, Casey BJ, Dubin MJ, Liston C. 2017. Resting-state connectivity
1166 biomarkers define neurophysiological subtypes of depression. Nat Med
1167 23:28–38. doi:10.1038/nm.4246

1168 Dube C, Chen K, Eghbal-Ahmadi M, Brunson K, Soltesz I, Baram TZ. 2000.
1169 Prolonged Febrile Seizures in the Immature Rat Model Enhance
1170 Hippocampal Excitability Long Term, Ann Neurol.

1171 Dubé C, Richichi C, Bender RA, Chung G, Litt B, Baram TZ. 2006a. Temporal
1172 lobe epilepsy after experimental prolonged febrile seizures: Prospective
1173 analysis. *Brain* **129**:911–922. doi:10.1093/brain/awl018

1174 Dubé C, Richichi C, Bender RA, Chung G, Litt B, Baram TZ. 2006b. Temporal
1175 lobe epilepsy after experimental prolonged febrile seizures: Prospective
1176 analysis. *Brain* **129**:911–922. doi:10.1093/brain/awl018

1177 Dzirasa K, Ribeiro S, Costa R, Santos LM, Lin SC, Grosmark A, Sotnikova TD,
1178 Gainetdinov RR, Caron MG, Nicolelis MAL. 2006. Dopaminergic control of
1179 sleep-wake states. *Journal of Neuroscience* **26**:10577–10589.
1180 doi:10.1523/JNEUROSCI.1767-06.2006

1181 Ellenbroek BA, Cools AR. 2002. Apomorphine Susceptibility and Animal Models
1182 for Psychopathology: Genes and Environment, Behavior Genetics.

1183 Ey E, Leblond CS, Bourgeron T. 2011. Behavioral profiles of mouse models for
1184 autism spectrum disorders. *Autism Research*. doi:10.1002/aur.175

1185 Floresco SB, Seamans JK, Phillips AG. 1997. Selective Roles for Hippocampal,
1186 Prefrontal Cortical, and Ventral Striatal Circuits in Radial-Arm Maze Tasks
1187 With or Without a Delay.

1188 Gao R, Peterson EJ, Voytek B. 2017. Inferring synaptic excitation/inhibition
1189 balance from field potentials. *Neuroimage* **158**:70–78.
1190 doi:10.1016/j.neuroimage.2017.06.078

1191 Garcia-Alvarez G, Shetty MS, Lu B, Yap KAF, Oh-Hora M, Sajikumar S, Bichler
1192 Z, Fivaz M. 2015. Impaired spatial memory and enhanced long-term
1193 potentiation in mice with forebrain-specific ablation of the Stim genes. *Front*
1194 *Behav Neurosci* **9**. doi:10.3389/fnbeh.2015.00180

1195 Gervasoni D, Lin SC, Ribeiro S, Soares ES, Pantoja J, Nicolelis MAL. 2004.
1196 Global forebrain dynamics predict rat behavioral states and their transitions.
1197 *Journal of Neuroscience* **24**:11137–11147. doi:10.1523/JNEUROSCI.3524-
1198 04.2004

Gomes F V., Zhu X, Grace AA. 2020. Correction: The pathophysiological impact of stress on the dopamine system is dependent on the state of the critical period of vulnerability (Molecular Psychiatry, (2020), 25, 12, (3278-3291), 10.1038/s41380-019-0514-1). Mol Psychiatry. doi:10.1038/s41380-019-0527-9

Goto Y, Grace AA. 2006. Alterations in Medial Prefrontal Cortical Activity and Plasticity in Rats with Disruption of Cortical Development. *Biol Psychiatry* **60**:1259–1267. doi:10.1016/j.biopsych.2006.05.046

Grace AA. 2016. Dysregulation of the dopamine system in the pathophysiology of schizophrenia and depression. *Nat Rev Neurosci*. doi:10.1038/nrn.2016.57

Holmes GL. 2016. Effect of Seizures on the Developing Brain and Cognition. *Semin Pediatr Neurol*. doi:10.1016/j.spen.2016.05.001

Holmes GL. 2009. The Long-Term Effects of Neonatal Seizures. *Clin Perinatol*. doi:10.1016/j.clp.2009.07.012

Holmes GL, Tian C, Hernan AE, Flynn S, Camp D, Barry J. 2015. Alterations in sociability and functional brain connectivity caused by early-life seizures are prevented by bumetanide. *Neurobiol Dis* **77**:204–219. doi:10.1016/j.nbd.2015.02.015

Johnson RA, Wichern DW. 2007. Applied Multivariate Statistical Analysis, 6th ed. Pearson Prentice Hall.

Kandratavicius L, Lopes-Aguiar C, Bueno-Júnior LS, Romcy-Pereira RN, Hallak JEC, Leite JP. 2012a. Comorbidades psiquiátricas na epilepsia do lobo temporal: Possíveis relações entre desordens psicóticas e comprometimento de circuitos límbicos. *Revista Brasileira de Psiquiatria* **34**:454–466. doi:10.1016/j.rbp.2012.04.007

Kandratavicius L, Ruggiero RN, Hallak JE, Garcia-Cairasco N, Leite JP. 2012b. Pathophysiology of mood disorders in temporal lobe epilepsy. *Revista Brasileira de Psiquiatria* **34**:233–259. doi:10.1016/j.rbp.2012.08.003

Kaufmann R, Goldberg-Stern H, Shuper A. 2009. Attention-deficit disorders and epilepsy in childhood: Incidence, causative relations and treatment possibilities. *J Child Neurol*. doi:10.1177/0883073808330165

Kleen JK, Wu EX, Holmes GL, Scott RC, Lenck-Santini PP. 2011. Enhanced oscillatory activity in the hippocampal-prefrontal network is related to short-term memory function after early-life seizures. *Journal of Neuroscience* **31**:15397–15406. doi:10.1523/JNEUROSCI.2196-11.2011

Kloc ML, Chen Y, Daglian JM, Holmes GL, Baram TZ, Barry JM. 2023. Spatial learning impairments and discoordination of entorhinal-hippocampal circuit coding following prolonged febrile seizures. *Hippocampus*. doi:10.1002/hipo.23541

1239 Kollins SH, Adcock RA. 2014. ADHD, altered dopamine neurotransmission, and
1240 disrupted reinforcement processes: Implications for smoking and nicotine
1241 dependence. *Prog Neuropsychopharmacol Biol Psychiatry*.
1242 doi:10.1016/j.pnpbp.2014.02.002

1243 Kosillo P, Bateup HS. 2021. Dopaminergic Dysregulation in Syndromic Autism
1244 Spectrum Disorders: Insights From Genetic Mouse Models. *Front Neural*
1245 *Circuits*. doi:10.3389/fncir.2021.700968

1246 Kubová H, Mareš P. 2013. Are morphologic and functional consequences of
1247 status epilepticus in infant rats progressive? *Neuroscience* **235**:232–249.
1248 doi:10.1016/j.neuroscience.2012.12.055

1249 Kubova H, Mares P, Suchomelova Â L, Ïek GB, Druga R, Pitka A, Nen È. 2004.
1250 Status epilepticus in immature rats leads to behavioural and cognitive
1251 impairment and epileptogenesis. *Eur J Neurosci* **19**:3255–65.
1252 doi:10.1111/j.1460-9568.2004.03410.x

1253 Laurence JA, Fatemi SH. 2005. Glial fibrillary acidic protein is elevated in superior
1254 frontal, parietal and cerebellar cortices of autistic subjects. *Cerebellum*
1255 **4**:206–210. doi:10.1080/14734220500208846

1256 Lesting J, Daldrup T, Narayanan V, Himpe C, Seidenbecher T, Pape HC. 2013.
1257 Directional Theta Coherence in Prefrontal Cortical to Amygdalo-Hippocampal
1258 Pathways Signals Fear Extinction. *PLoS One* **8**.
1259 doi:10.1371/journal.pone.0077707

1260 Lin TC, Huang LT, Huang YN, Chen GS, Wang JY. 2009. Neonatal status
1261 epilepticus alters prefrontal-striatal circuitry and enhances
1262 methamphetamine-induced behavioral sensitization in adolescence.
1263 *Epilepsy and Behavior* **14**:316–323. doi:10.1016/j.yebeh.2008.12.005

1264 Lopes-Aguiar C, Ruggiero RN, Rossignoli MT, Esteves I de M, Peixoto-Santos
1265 JE, Romcy-Pereira RN, Leite JP. 2020. Long-term potentiation prevents
1266 ketamine-induced aberrant neurophysiological dynamics in the
1267 hippocampus-prefrontal cortex pathway in vivo. *Sci Rep* **10**.
1268 doi:10.1038/s41598-020-63979-5

1269 Marín O. 2016. Developmental timing and critical windows for the treatment of
1270 psychiatric disorders. *Nat Med*. doi:10.1038/nm.4225

1271 Marques DB, Rossignoli MT, de Avó Mesquita B, Prizon T, Zacharias LR,
1272 Ruggiero RN, Leite JP. 2023. Decoding Fear or Safety and Approach or
1273 Avoidance by Brain-Wide Network Dynamics. bioRxiv.
1274 doi:10.1101/2022.10.13.511989

1275 Marques DB, Ruggiero RN, Bueno-Junior LS, Rossignoli MT, Leite JP. 2022.
1276 Prediction of Learned Resistance or Helplessness by Hippocampal-
1277 Prefrontal Cortical Network Activity during Stress. *Journal of Neuroscience*
1278 **42**:81–96. doi:10.1523/JNEUROSCI.0128-21.2021

1279 Meng Y, Zhang Y, Tregoubov V, Janus C, Cruz L, Jackson M, Lu W-Y,
1280 Macdonald JF, Wang JY, Falls DL, Jia Z. 2002. Abnormal Spine Morphology
1281 and Enhanced LTP in LIMK-1 Knockout Mice. Neuron.

1282 Minamiura Y, Hirayama K, Murata R, Matsuura S. 1996. Effect of hyperthermia
1283 on hippocampal synaptic transmission and CA3 kindling in developing rats,
1284 Brain Research.

1285 Mouchati PR, Barry JM, Holmes GL. 2019. Functional brain connectivity in a
1286 rodent seizure model of autistic-like behavior. *Epilepsy and Behavior* **95**:87–
1287 94. doi:10.1016/j.yebeh.2019.03.046

1288 Navakkode S, Zhai J, Wong YP, Li G, Soong TW. 2022. Enhanced long-term
1289 potentiation and impaired learning in mice lacking alternative exon 33 of
1290 CaV1.2 calcium channel. *Transl Psychiatry* **12**. doi:10.1038/s41398-021-
1291 01683-2

1292 Newson JJ, Thiagarajan TC. 2019. EEG Frequency Bands in Psychiatric
1293 Disorders: A Review of Resting State Studies. *Front Hum Neurosci*.
1294 doi:10.3389/fnhum.2018.00521

1295 Niedecker RW, Kloc ML, Holmes GL, Barry JM. 2021. Effects of early life seizures
1296 on coordination of hippocampal–prefrontal networks: Influence of sex and
1297 dynamic brain states. *Epilepsia* **62**:1701–1714. doi:10.1111/epi.16927

1298 Notenboom RGE, Ramakers GMJ, Kamal A, Spruijt BM, De Graan PNE. 2010.
1299 Long-lasting modulation of synaptic plasticity in rat hippocampus after early-
1300 life complex febrile seizures. *European Journal of Neuroscience* **32**:749–758.
1301 doi:10.1111/j.1460-9568.2010.07321.x

1302 Nuytens K, Gantois I, Stijnen P, Iscru E, Laeremans A, Serneels L, Van Eylen L,
1303 Liebhaber SA, Devriendt K, Balschun D, Arckens L, Creemers JWM,
1304 D'Hooge R. 2013. Haploinsufficiency of the autism candidate gene
1305 Neurobeachin induces autism-like behaviors and affects cellular and
1306 molecular processes of synaptic plasticity in mice. *Neurobiol Dis* **51**:144–151.
1307 doi:10.1016/j.nbd.2012.11.004

1308 O'Leary H, Bernard PB, Castano AM, Benke TA. 2016. Enhanced long term
1309 potentiation and decreased AMPA receptor desensitization in the acute
1310 period following a single kainate induced early life seizure. *Neurobiol Dis*
1311 **87**:134–144. doi:10.1016/j.nbd.2015.12.005

1312 Otani S, Bai J, Blot K. 2015. Dopaminergic modulation of synaptic plasticity in rat
1313 prefrontal neurons. *Neurosci Bull*. doi:10.1007/s12264-014-1507-3

1314 Ozaki N, Nakahara T, Miura H, Kasahara Y, Nagatsu S. 1989. Effects of
1315 Apomorphine on In Vivo Release of Dopamine and Its Metabolites in the
1316 Prefrontal Cortex and the Striaturn, Studied by a Microdialysis Method, J.
1317 Neurochem.

1318 Peixoto-Santos JE, Velasco TR, Galvis-Alonso OY, Araujo D, Kandratavicius L,
1319 Assirati JA, Carlotti CG, Scandiuzzi RC, Dos Santos AC, Leite JP. 2015.

1320 Temporal lobe epilepsy patients with severe hippocampal neuron loss but
1321 normal hippocampal volume: Extracellular matrix molecules are important for
1322 the maintenance of hippocampal volume. *Epilepsia* **56**:1562–1570.
1323 doi:10.1111/epi.13082

1324 Prata J, Santos SG, Almeida MI, Coelho R, Barbosa MA. 2017. Bridging Autism
1325 Spectrum Disorders and Schizophrenia through inflammation and
1326 biomarkers - pre-clinical and clinical investigations. *J Neuroinflammation*.
1327 doi:10.1186/s12974-017-0938-y

1328 Racine RJ. 1971. Electroencephalography and Clinical Neurophysiology
1329 MODIFICATION OF SEIZURE ACTIVITY BY ELECTRICAL STIMULATION:
1330 II. MOTOR SEIZURE. *Electroencephalogr Clin Neurophysiol* **32.**:281–94.

1331 Regan SL, Williams MT, Vorhees C V. 2022. Review of rodent models of attention
1332 deficit hyperactivity disorder. *Neurosci Biobehav Rev*.
1333 doi:10.1016/j.neubiorev.2021.11.041

1334 Rojas DC, Wilson LB. 2014. γ-band abnormalities as markers of autism spectrum
1335 disorders. *Biomark Med*. doi:10.2217/bmm.14.15

1336 Ruggiero RN, Lopes-Aguiar C, Leite JP. 2012. Early Life Seizures and Their
1337 Long-term Impacts on Cognition: The Role of Synaptic Plasticity
1338 Dysfunctions as an Underlying Mechanism. *Journal of epilepsy and clinical*
1339 *neurophysiology.*

1340 Ruggiero RN, Rossignoli MT, Lopes-Aguiar C, Leite JP, Bueno-Junior LS,
1341 Romcy-Pereira RN. 2018. Lithium modulates the muscarinic facilitation of
1342 synaptic plasticity and theta-gamma coupling in the hippocampal-prefrontal
1343 pathway. *Exp Neurol* **304**:90–101. doi:10.1016/j.expneurol.2018.02.011

1344 Ruggiero RN, Rossignoli MT, Marques DB, de Sousa BM, Romcy-Pereira RN,
1345 Lopes-Aguiar C, Leite JP. 2021. Neuromodulation of Hippocampal-Prefrontal
1346 Cortical Synaptic Plasticity and Functional Connectivity: Implications for
1347 Neuropsychiatric Disorders. *Front Cell Neurosci*.
1348 doi:10.3389/fncel.2021.732360

1349 Scott KE, Schormans AL, Pacoli KY, De Oliveira C, Allman BL, Schmid S. 2018.
1350 Altered auditory processing, filtering, and reactivity in the cntnap2 knock-out
1351 rat model for neurodevelopmental disorders. *Journal of Neuroscience*
1352 **38**:8588–8604. doi:10.1523/JNEUROSCI.0759-18.2018

1353 Short AK, Baram TZ. 2019. Early-life adversity and neurological disease: age-old
1354 questions and novel answers. *Nat Rev Neurol*. doi:10.1038/s41582-019-
1355 0246-5

1356 Sigurdsson T. 2016. Neural circuit dysfunction in schizophrenia: Insights from
1357 animal models. *Neuroscience*. doi:10.1016/j.neuroscience.2015.06.059

1358 Sigurdsson T, Duvarci S. 2016. Hippocampal-prefrontal interactions in cognition,
1359 behavior and psychiatric disease. *Front Syst Neurosci*.
1360 doi:10.3389/fnsys.2015.00190

1361 Sinh Y, Raol H, Budreck EC, Brooks-Kayal AR. 2003. Epilepsy after Early-Life
1362 Seizures Can Be Independent of Hippocampal Injury, Ann Neurol.

1363 Somera-Molina KC, Robin B, Somera CA, Anderson C, Stine C, Koh S, Behanna
1364 HA, Van Eldik LJ, Watterson DM, Wainwright MS. 2007. Glial activation links
1365 early-life seizures and long-term neurologic dysfunction: Evidence using a
1366 small molecule inhibitor of proinflammatory cytokine upregulation. *Epilepsia*
1367 **48**:1785–1800. doi:10.1111/j.1528-1167.2007.01135.x

1368 Thörn CW, Kafetzopoulos V, Kocsis B. 2022. Differential Effect of Dopamine D4
1369 Receptor Activation on Low-Frequency Oscillations in the Prefrontal Cortex
1370 and Hippocampus May Bias the Bidirectional Prefrontal–Hippocampal
1371 Coupling. *Int J Mol Sci* **23**. doi:10.3390/ijms231911705

1372 Tsai ML, Crutchley M, Boyce R, Ma J, Boon F, Cain DP, Leung LS. 2012. Long-
1373 lasting auditory gating deficit accompanied by GABA B receptor dysfunction
1374 in the hippocampus after early-life limbic seizures in rats. *Physiol Behav*
1375 **106**:534–541. doi:10.1016/j.physbeh.2012.03.033

1376 Turetsky BI, Calkins ME, Light GA, Olincy A, Radant AD, Swerdlow NR. 2007.
1377 Neurophysiological endophenotypes of schizophrenia: The viability of
1378 selected candidate measures. *Schizophr Bull*. doi:10.1093/schbul/sbl060

1379 Uhlhaas PJ, Singer W. 2012. Neuronal dynamics and neuropsychiatric disorders:
1380 toward a translational paradigm for dysfunctional large-scale networks.
1381 Neuron. Sep 20;75(6):963-80. doi: 10.1016/j.neuron.2012.09.004. PMID:
1382 22998866.

1383 Velasquez F, Dickson C, Kloc ML, Schneur CA, Barry JM, Holmes GL. 2023.
1384 Optogenetic modulation of hippocampal oscillations ameliorates spatial
1385 cognition and hippocampal dysrhythmia following early-life seizures.
1386 *Neurobiol Dis* **178**. doi:10.1016/j.nbd.2023.106021

1387 Vezzani A, Aronica E, Mazarati A, Pittman QJ. 2013. Epilepsy and brain
1388 inflammation. *Exp Neurol*. doi:10.1016/j.expneurol.2011.09.033

1389 Wolf DC, Bueno-Júnior LS, Lopes-Aguiar C, Do Val Da Silva RA, Kandratavicius
1390 L, Leite JP. 2016. The frequency of spontaneous seizures in rats correlates
1391 with alterations in sensorimotor gating, spatial working memory, and
1392 parvalbumin expression throughout limbic regions. *Neuroscience* **312**:86–98.
1393 doi:10.1016/j.neuroscience.2015.11.008

1394 Yokoi F, Chen HX, Dang MT, Cheetham CC, Campbell SL, Roper SN, Sweatt
1395 JD, Li Y. 2015. Behavioral and electrophysiological characterization of Dyt1
1396 heterozygous knockout mice. *PLoS One* **10**.
1397 doi:10.1371/journal.pone.0120916

1398 Ziermans T, Schothorst P, Magnée M, van Engeland H, Kemner C. 2011.
1399 Reduced prepulse inhibition in adolescents at risk for psychosis: A 2-year
1400 follow-up study. *Journal of Psychiatry and Neuroscience* **36**:127–134.
1401 doi:10.1503/jpn.100063

Figures and Legends

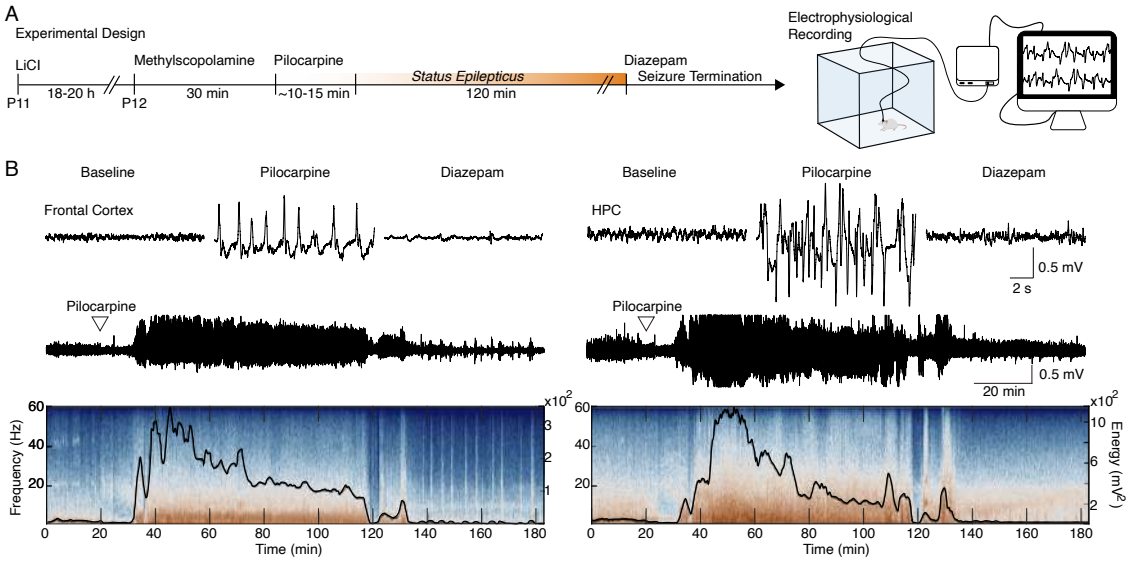

Figure 1. ELS induction. *A,* Experimental design representing early-life SE induction and monitoring. ***B,*** Representative traces of LFP during baseline, motor seizure induced by pilocarpine, and ELS interruption with diazepam injection (top). Representative LFP from the frontal cortex and HPC throughout the experiment (middle). LFPs are aligned with their respective spectrograms and energy curves (bottom). ELS n=5.

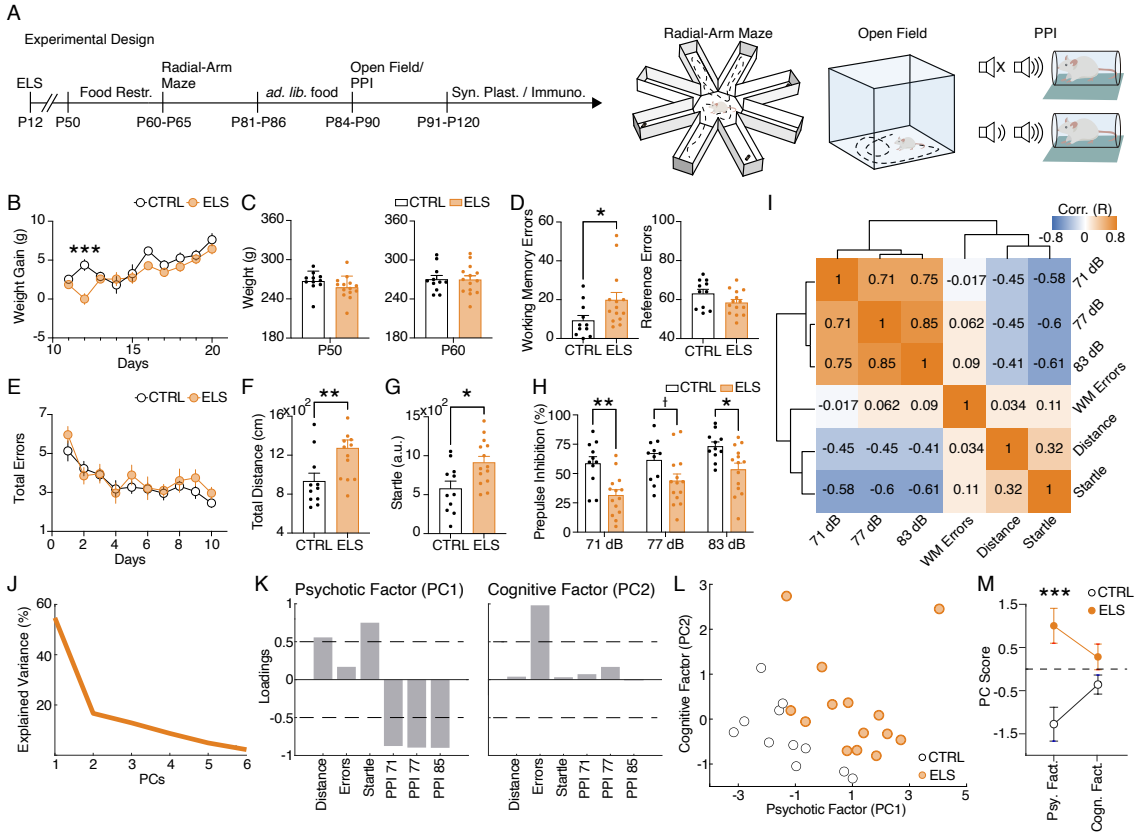

Figure 2. ELS induces cognitive and sensorimotor impairments. *A,* Experimental design representing early-life SE induction, age of the animals during the experiments, and behavioral tests performed. ***B,*** Weight gain after ELS induction. ELS rats showed weight loss only on the ELS induction day. ***C,*** No weight differences between ELS and CTRL throughout experiments in adulthood, regardless if before food restriction (left) or during food restriction (right). ***D,*** Working memory task on the radial-arm maze. ***E,*** ELS rats showed an increase in working memory errors across sessions (left) without differences in the number of reference errors (right). E, ELS rats showed a similar learning curve when compared to CTRL. ***F,*** Hyperlocomotion of ELS rats in the open field test. ***G,*** Higher acoustic startle of ELS rats. ***H,*** Impaired sensorimotor gating in ELS rats as measured in the PPI test with three stimulus intensities. ***I,*** Correlation matrix of all behavioral variables. Note a cluster of positive correlations formed by the PPI measures and another cluster of negative correlations formed by the PPI measures with distance traveled on the open field and the acoustic startle. Working memory errors were not correlated with the other behavioral features. ***J,*** Explained variance from principal components analysis (PCA). Note that the two first PCs explain 71.32% of the data. ***K,*** Loadings of the behavioral variables on each principal component (PC) reveal a *sensorimotor factor* (PC1) and an uncorrelated *cognitive factor* (PC2). ***L,*** PCA of the behavioral features showing each animal projected onto the new factors. ***M,*** The sensorimotor factor distinguishes ELS from CTRL animals, as we compare the PC scores from each group. † $p < 0.1$, *$p < 0.05$, **$p < 0.01$, ***$p < 0.001$. CTRL n=11, and ELS n=14. Error bars represent the mean ± SEM.

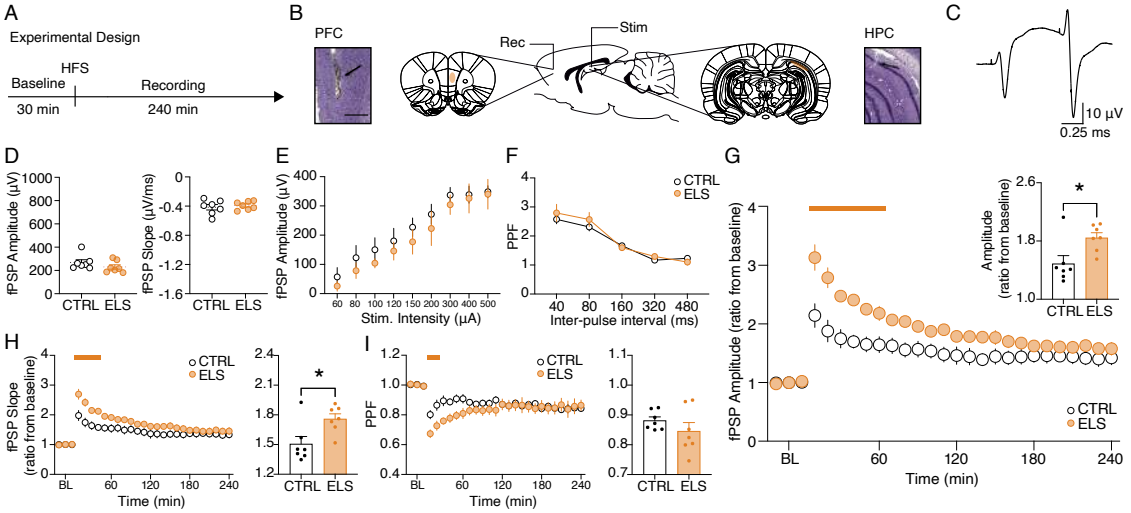

Figure 3. Aberrant HPC-PFC synaptic plasticity in animals submitted to ELS. *A,* Experimental design including high-frequency stimulation (HFS) to LTP induction. ***B,*** Electrode placement and representative electrolytic lesions in Cresyl Violet stained coronal sections. ***C,*** Representative evoked fPSPs in the PFC. No difference between ELS and CTRL rats in terms of basal neurotransmission and synaptic efficacy, as shown by: ***(D)***, fPSP amplitude (left) and slope (right); ***(E),*** input-output curve; and ***(F),*** paired-pulse facilitation (PPF) curve. ***G,*** Despite no changes in basal synaptic efficacy, ELS rats showed aberrantly increased LTP, represented by higher fPSP amplitude ratios from baseline (BL) post-HFS, both across time blocks (main curve graph) and their averages (bar graph, inset). ***H,*** As in ***G,*** but from fPSP slopes. ***I,*** ELS rats showed reduced PPF in the initial 30 min (curve graph). Averaged data resulted in no differences between the groups (bar graph, inset). † $p < 0.1$, *$p < 0.05$, **$p < 0.01$, ***$p < 0.001$. CTRL n=7, and ELS n=7. Error bars represent the mean ± SEM.

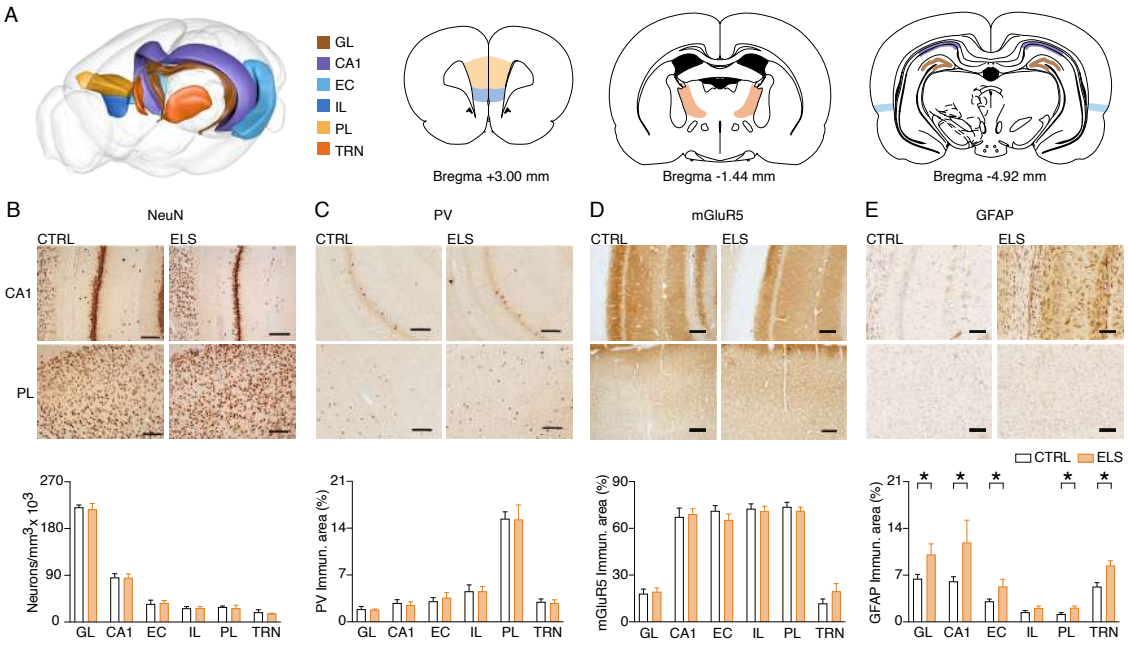

Figure 4. ELS induces long-term neural inflammation, but not neuronal loss. *A* 3-D brain diagram and coronal sections representing the brain regions investigated. ***B-E***, Representative photomicrographs from immunohistochemistry each pair of columns represents a group comparison (left CTRL and right ELS) and each line is related to CA1 and PL, respectively. ***B,*** NeuN immunohistochemistry showing that ELS rats did not present neuronal loss. ***C,*** Parvalbumin (PV) immunohistochemistry. ***D,*** mGluR5: ***E***, GFAP, showing increased astrogliosis induced by ELS. GL: Granule layer of dentate gyrus; CA1: *Cornu Ammonis* 1; EC: Entorhinal cortex; IL: Infralimbic cortex; PL: Prelimbic cortex; TRN: Thalamic Reticular Nucleus. *$p < 0.05$. CTRL n=11, and ELS n=14. Error bars represent the mean ± SEM.

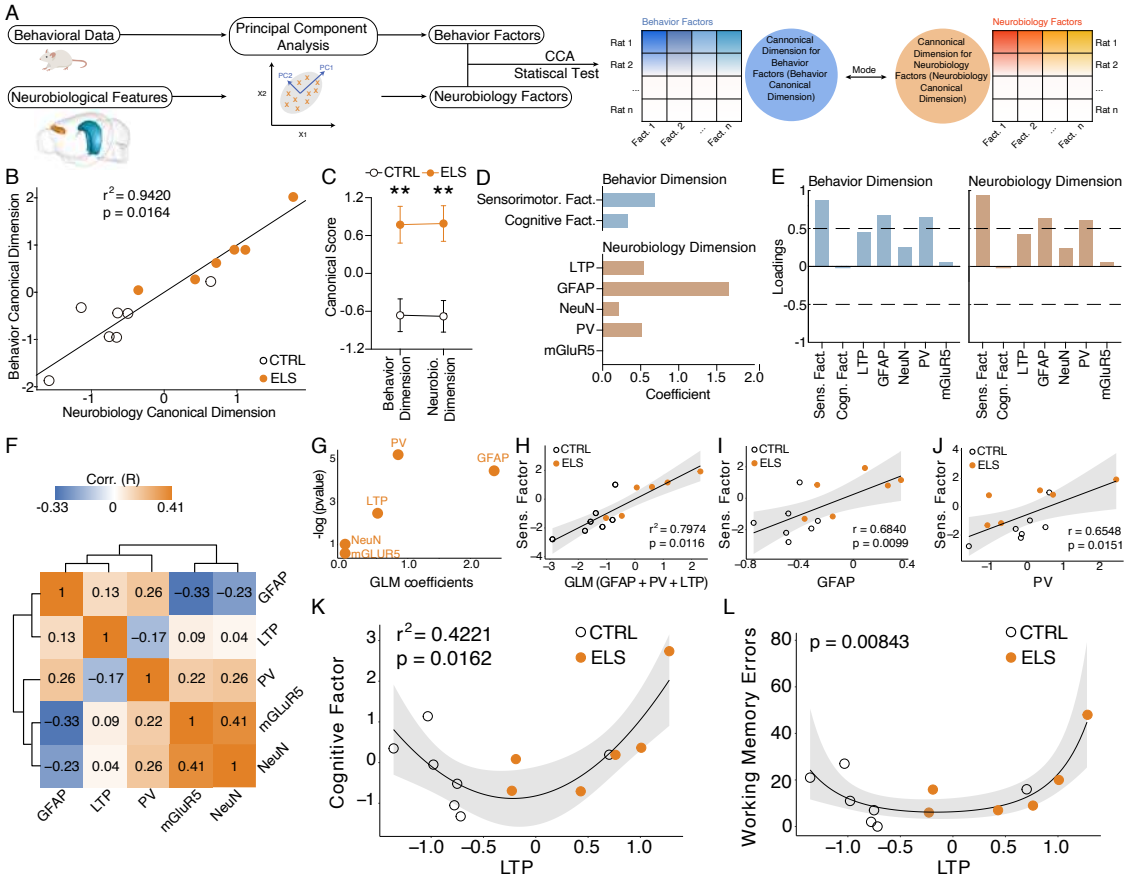

Figure 5. Cognitive impairment and sensorimotor deficits are distinctly correlated with abnormal LTP and neuroinflammation. ***A,*** Steps performed in data processing and analysis for canonical correlation analysis (CCA). ***B,*** CCA analysis showing CTRL and ELS animals projected onto the first canonical correlation. We found a strong correlation between the neurobiology canonical dimension and the behavior canonical dimension. ***C,*** Canonical scores showing the clear CTRL *vs.* ELS difference that the CCA was able to capture. ***D,*** Coefficients for behavior and neurobiology canonical dimensions, showing greater contributions of the sensorimotor factor, GFAP, PV, and LTP for the correlation. ***E,*** Loadings of the behavioral and neurobiological variables on each canonical correlation dimension indicating an association between GFAP and PV with the sensorimotor factor. ***F,*** Correlation matrix showing only weak correlations between the neurobiological features. ***G,*** GLM regression between neurobiological features and the sensorimotor factor. ***H***, GLM model between neurobiological features and the sensorimotor factor show a strong association with GFAP, PV, and LTP. ***I,*** GLM regression between LTP and the cognitive factor shows a quadratic association (left). This quadratic association was further confirmed performing a quasi-Poisson regression between LTP and raw values of working memory errors (right). **$p < 0.01$. CTRL n=7, and ELS n=6. Error bars represent the mean ± SEM.

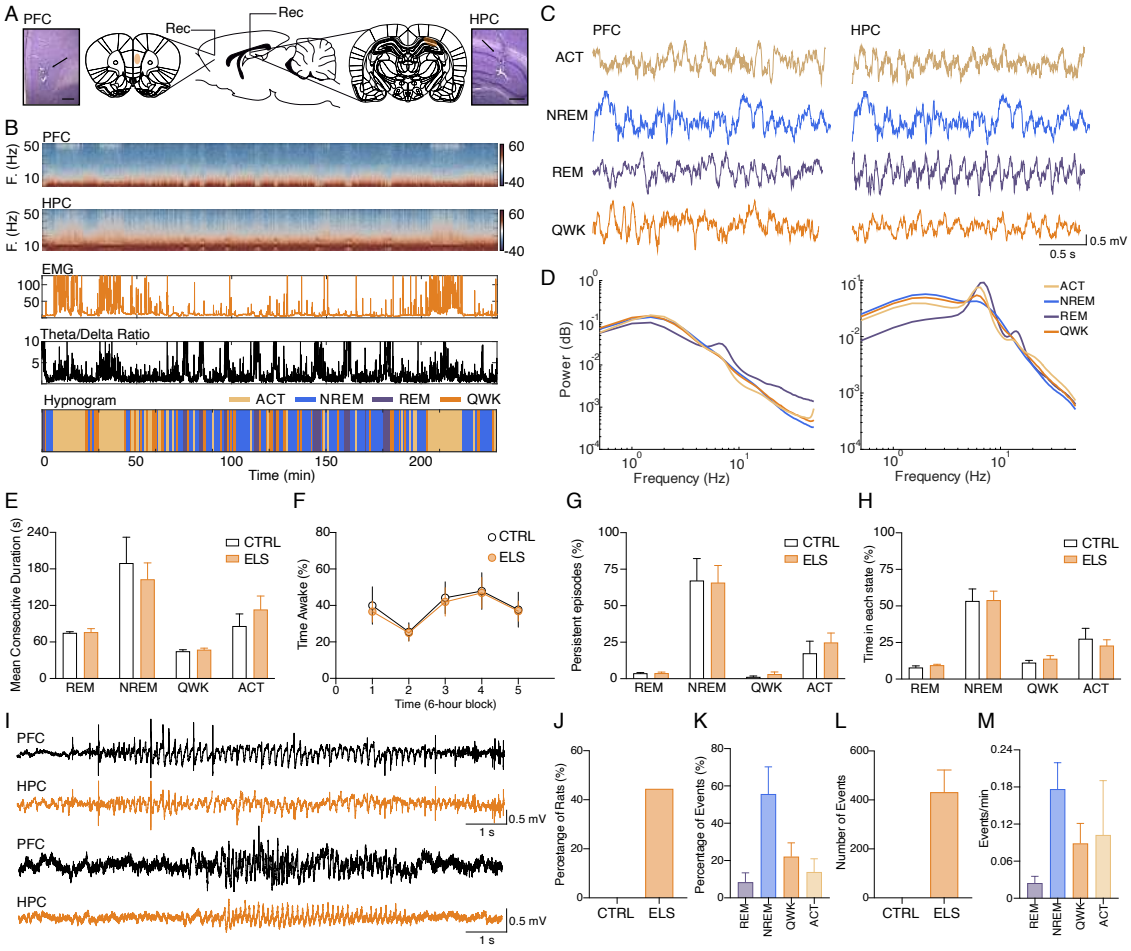

Figure 6. Classification of sleep-wake states and electrographic discharges in ELS rats. *A,* Electrode placement and representative electrolytic lesions in Nissl-stained coronal sections. ***B,*** Representative spectrogram, electromyogram (EMG) root mean squared (RMS), and HPC theta/delta ratio used to score the sleep-wake cycle and to generate the hypnogram (bottom). ***C,*** Representative LFPs (top) recorded from PFC and HPC during ACT, NREM, REM, and QWK. ***D,*** Average power spectral density for each state in the PFC and HPC of a representative CTRL animal. Note the increase in HPC theta power during ACT and REM. ELS rats did not present alterations in the sleep-wake cycle. ***E-H***, There were no differences between ELS and CTRL in the ***(E)*** Mean duration of consecutive epochs for each state, ***(F)*** percentage of time awake across 6-h blocks, and in the ***(G)*** number of persistent episodes (episodes lasting longer than 3 s, top) or the ***(H)*** percentage of time spent in each state (bottom). ***I,*** Representative LFP from PFC and HPC showing a representative spike-wave discharge (SWD, top) and a poly-spike discharge (bottom). ***J,*** Electrographic discharges were found in 44.5% of ELS animals and were absent in CTRL animals. ***K,*** Percentage of events occurring in each sleep-wake stage. ***L,*** Average total number of SWD events in CTRL and ELS animals. ***M,*** Frequency of SWDs occurring per state. SWDs events rarely occurred during REM. CTRL n=6, and ELS n=9. Error bars represent the mean ± SEM.

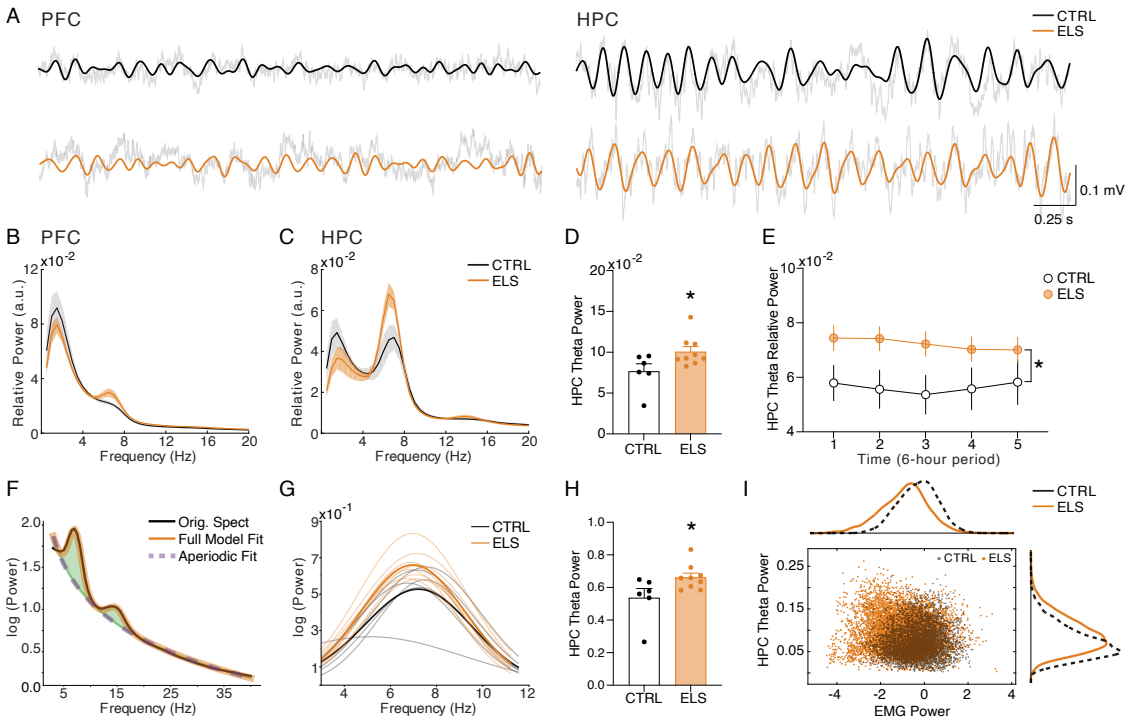

Figure 7. Increased HPC theta power during behavioral activity in ELS animals. *A,* Representative raw LFPs (transparent black lines) and theta-filtered signal of CTRL (black) and ELS (orange) from the PFC (left) and HPC (right) during ACT. ***B,*** Relative PSD of the PFC during ACT. ***C,*** Relative PSD of the HPC during ACT. ***D,*** ELS rats present an enhanced HPC theta power during ACT. ***E,*** Theta relative power during each of the 6-hour periods of recording, showing a general increase in the ELS animals that is more pronounced in the initial 18 h of recording. ***F,*** Parametric model used to distinguish oscillatory from aperiodic component. ***G,*** Oscillatory components extracted from ACT PSDs used to calculate theta power. ***H,*** Theta power increase in ELS rats is due to a true oscillatory component and not from the aperiodic activity in ACT states. ***I,*** Theta power increase in ELS rats is independent of locomotor activity. Note from the distribution of relative theta power and Z-scored EMG (trapezius) values for all rats that EMG power is not related to the regions of greater theta power in the ELS animals. *$p < 0.05$. CTRL n=6, and ELS n=9. Error bars represent the mean ± SEM.

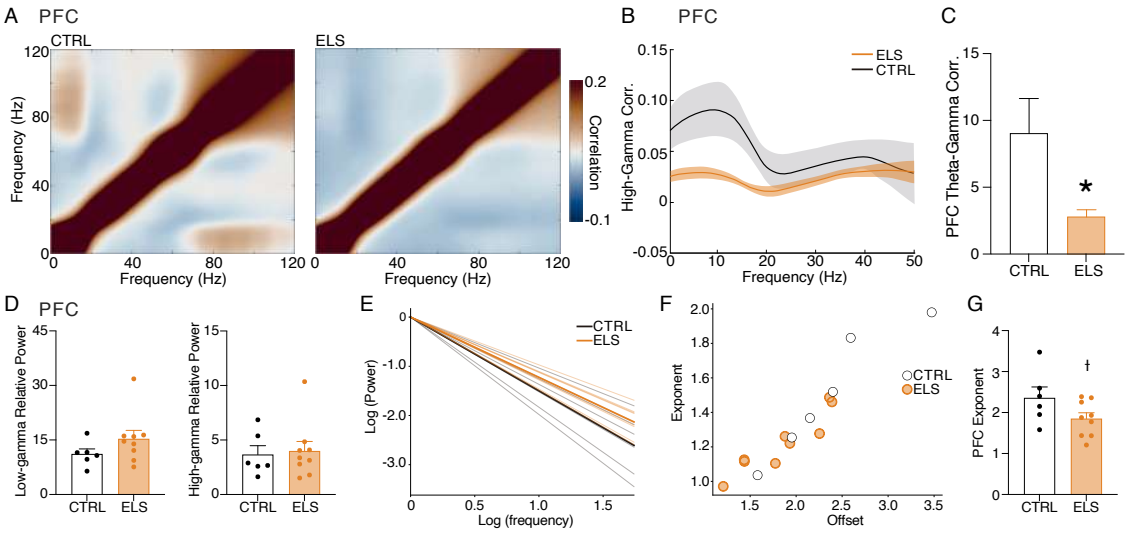

Figure 8. ELS promotes abnormal gamma coordination in the PFC during behavioral activity. ELS rats present an abnormal gamma activity in the PFC. ***A,*** Grand-average amplitude correlogram for CTRL (left) and ELS (right) group. Note the absence of amplitude correlation between theta and gamma activity in the ELS group. ***B,*** High-gamma (65-100 Hz) correlation with low-frequency activity. Note the peak around theta oscillation in the CTRL group and the absence in ELS. ***C,*** ELS present an impaired theta-gamma amplitude correlation. ***D,*** There is no difference between the low- (top) and high-gamma (bottom) average power. ***E,*** Aperiodic activity extracted from the PFC of each rat during ACT state. ***F,*** Distribution of the parameters of the aperiodic component (exponent and offset) for each rat. ***G,*** ELS rats show a tendency to reduction (p = 0.0656) in the exponent parameter of the aperiodic component, as illustrated by the flatter spectra. † $p < 0.1$, *$p < 0.05$. CTRL n=6, and ELS n=9. Error bars represent the mean ± SEM.

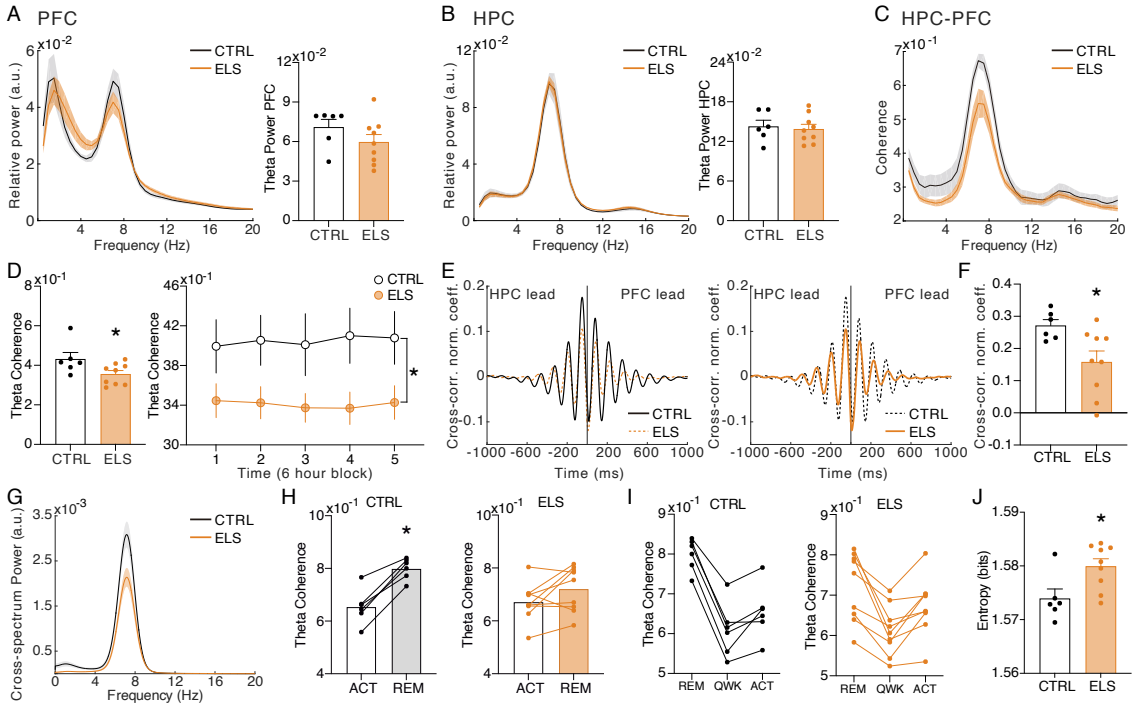

Figure 9. ELS impairs HPC-PFC coherence during REM sleep. *A,* PSD in the PFC during REM. ***B,*** PSD in the HPC during REM. No significant alterations in theta power during REM are observed in ELS rats. ***C,*** Theta coherence is diminished in ELS rats. ***D,*** Significant effect on the HPC-PFC theta coherence by averaging the entire recording (left) and across all periods (right). ***E,*** Time domain cross-correlation between PFC and HPC LFPs during REM epochs highlighting CTRL (left) and ELS (right) group averages. ***F,*** Reduction in the peak of correlation between -80 to -20 ms in ELS rats***. G,*** Average cross-spectrum power density showing a reduced theta peak in the ELS rats. ***H,*** Theta HPC-PFC coherence increases from ACT to REM states. We can observe that all the CTRL rats present an increase from ACT to REM, while in ELS rats this is not observed. Paired *t*-test *$p < 0.05$. ***I,*** Theta coherence dynamics across the sleep-wake cycle. CTRL rats display a homogeneous dynamics with theta coherence being maximal at REM, minimal in QWK, and intermediate in ACT states. This dynamic is disrupted in ELS rats that display a higher variance between animals, with some animals displaying similar coherence in REM and ACT. ***J,*** Entropy of the theta coherence dynamics is higher in ELS rats, representing the more homogeneous values across states. CTRL n=6, and ELS n=9.

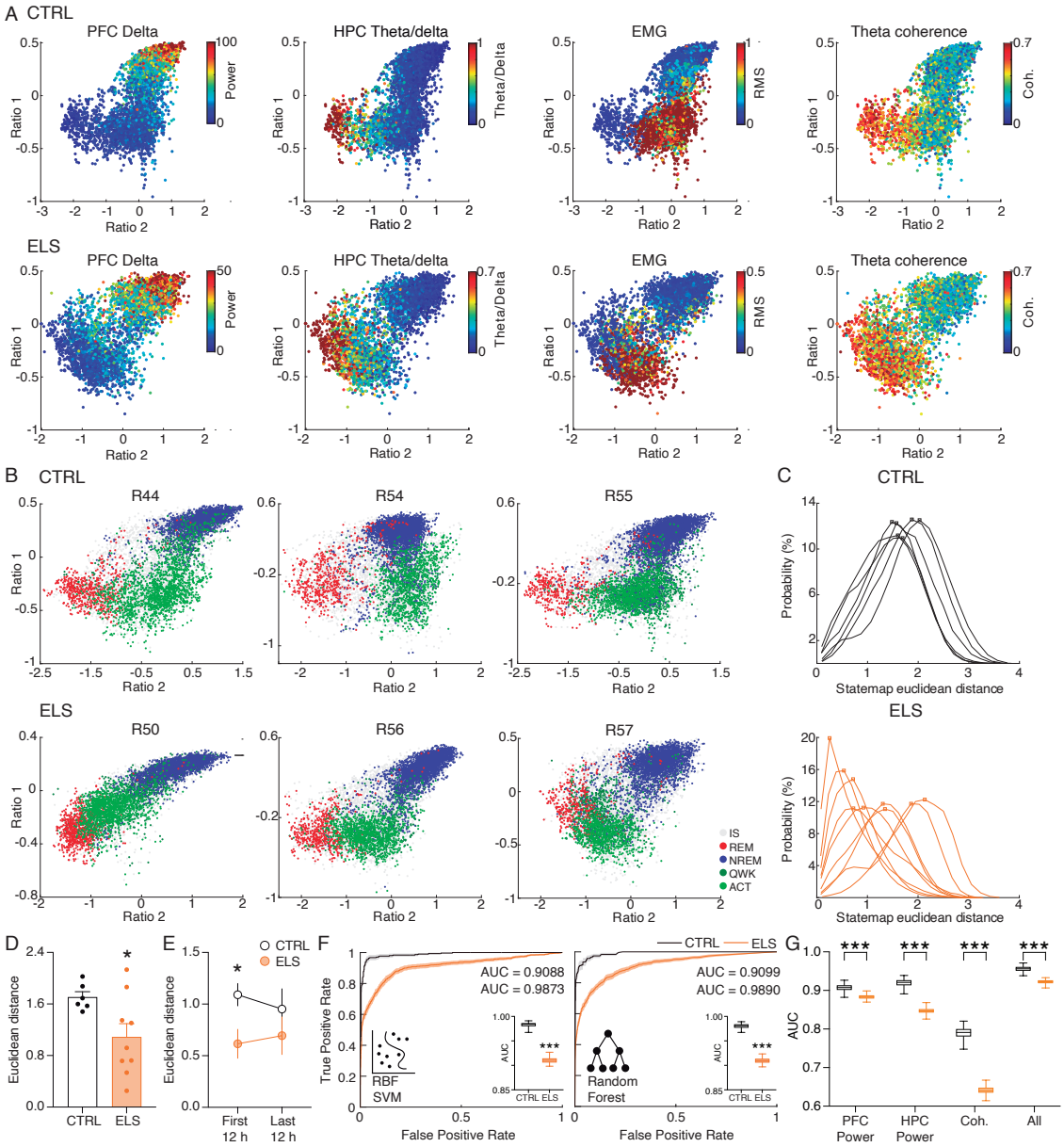

Figure 10. ELS rats display REM-like oscillatory dynamics during active behavior. *A,* State map construction reflects the sleep-wake cycle and spectral dynamics for one representative CTRL (top) and ELS (bottom) rat. PFC delta power is evident during NREM, theta/delta ratio is maximum in REM, EMG power describes ACT states, and HPC-PFC theta coherence is stronger close to REM. Note that in the ELS rat, the coherence is also broadly high during the ACT state. ***B,*** Representative state maps from three CTRL (top) and three ELS (bottom) rats. CTRL rats displayed a clear separation between REM (red), ACT (light green), and NREM (blue) clusters. ELS displayed an overlap between REM and ACT states. ***C,*** Distributions of the Euclidean distances between each REM and ACT epoch for CTRL (top) and ELS (bottom) rats. ELS distributions were heterogeneous, many of which were skewed to shorter distances. ***D,*** Average Euclidean distance showing that ELS rats have REM-like oscillatory dynamics during active behavior. ***E,*** REM-like oscillations during ACT were more pronounced in ELS during the initial 12 h of recording. ***F,*** Machine learning approach to decode REM *versus* ACT states. We used radial

basis function support vector machine (SVM) and random forest (RF) algorithm in order to classify REM and ACT epochs in CTRL (black) or ELS (orange) rats. Using a bootstrapped confidence interval, we observed that the discriminative performance was worse in ELS animals, even when using “brute-force” algorithms. ***G,*** A machine learning algorithm (random forest) fitted on whole-spectrum data also shows a significantly worse performance in ELS for PFC power, HPC power, coherence, and all estimates combined. † p < 0.1, *p < 0.05, **p < 0.01, ***p < 0.001. CTRL n=6, and ELS n=9. Error bars represent the mean ± SEM.

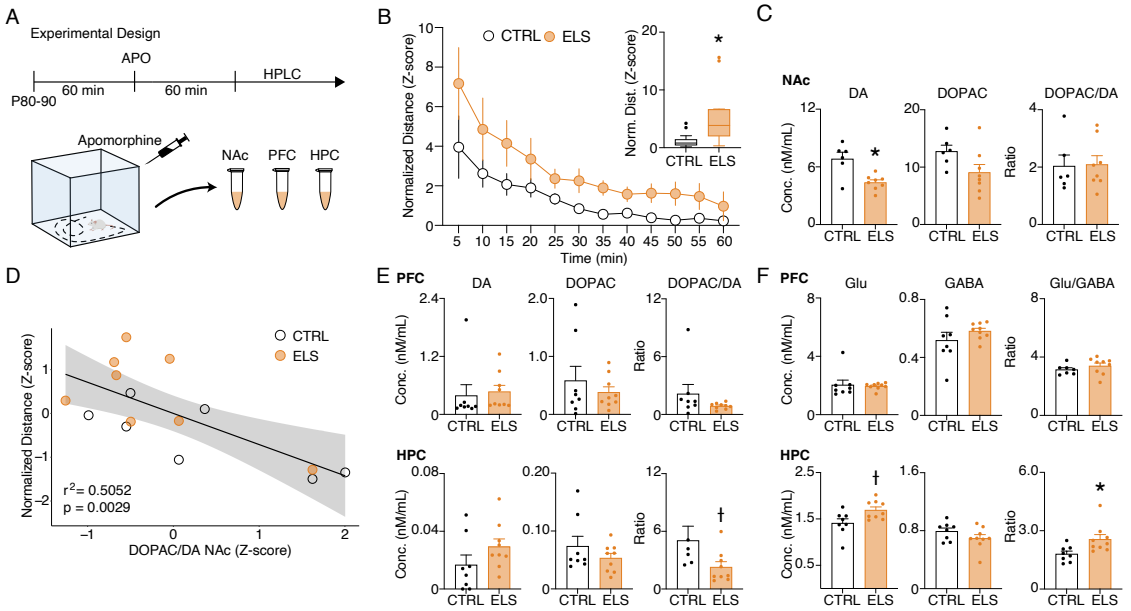

Figure 11. ELS rats present behavioral and neurochemical sensitivity to dopaminergic activation. ***A,*** Experimental design representing quantification of locomotion in the open field, apomorphine (APO) injection, and neurochemical analysis. ***B,*** Normalized locomotion across time blocks after APO injection, demonstrating increased locomotion of ELS rats induced by APO. Average normalized locomotion after APO injection (inset). *CTRL n=15, and ELS n=14.* ***C,*** Concentration of dopamine and metabolites in the NAc. ***D,*** GLM for the total distance after APO indicating DOPAC/DA ratio in the NAc as a strong significant variable associated with behavioral sensitivity to APO. ***E,*** Concentration of dopamine and metabolites (left) in the PFC (upper panel) and HPC (lower panel). Concentration of glutamate and GABA (right) in the PFC (upper panel) and HPC (lower panel). CTRL n=8, and ELS n=9. †Uncorrected p < 0.05, * multiple comparison corrected p < 0.05. Error bars represent the mean ± SEM.

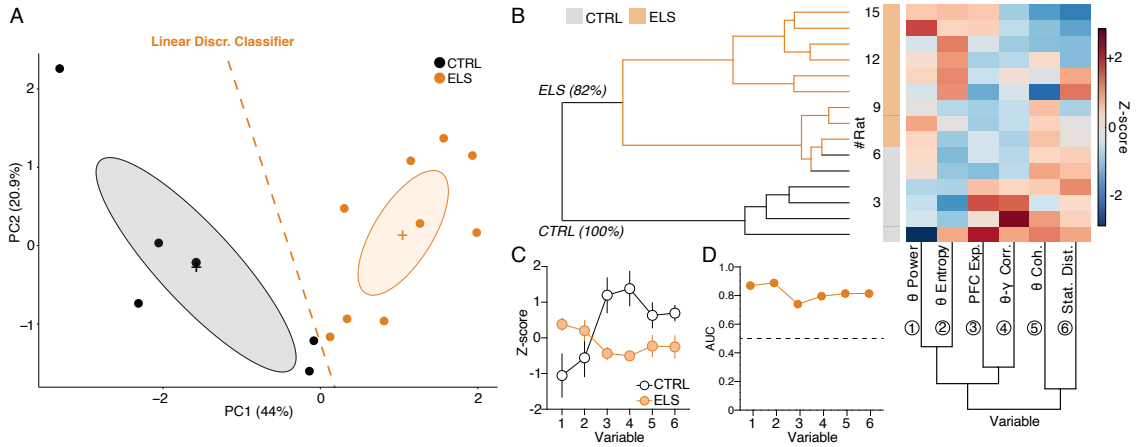

Figure 12. HPC and PFC oscillatory dynamics discriminate ELS rats. *A,* A linear discriminant classifier (dotted orange line) using the first two principal components (PCs) of relevant electrophysiological variables completely distinguishes ELS from CTRL rats (100% accuracy; 93.34% leave-one-out cross-validation). Note that the PC1 alone completely discriminates ELS rats. ***B,*** Unsupervised hierarchical clustering using the electrophysiological variables (bottom dendrogram) almost completely dissociates ELS from CTRL rats (left dendrogram). Inside the ELS cluster, we can observe one complete ELS branch, but the other overlapping with some CTRL animals, suggesting a graduality in the pathophysiological effects of ELS. ***C,*** Z-score values of each variable, showing distinct patterns of activity for each group. ***D,*** All the electrophysiological variables are good discriminators of CTRL and ELS rats (AUC-ROC > 0.7). † $p < 0.1$, *$p < 0.05$, **$p < 0.01$, ***$p < 0.001$. CTRL n=6, and ELS n=9. Error bars represent the mean ± SEM.